

Nanoscale

Accepted Manuscript



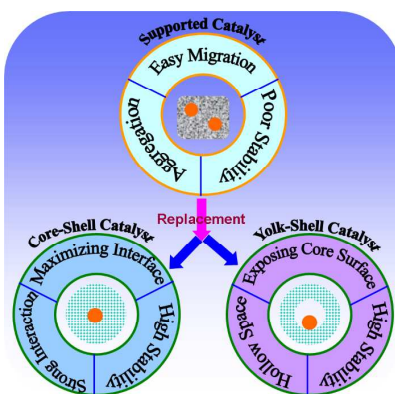
This is an *Accepted Manuscript*, which has been through the Royal Society of Chemistry peer review process and has been accepted for publication.

Accepted Manuscripts are published online shortly after acceptance, before technical editing, formatting and proof reading. Using this free service, authors can make their results available to the community, in citable form, before we publish the edited article. We will replace this *Accepted Manuscript* with the edited and formatted *Advance Article* as soon as it is available.

You can find more information about *Accepted Manuscripts* in the [Information for Authors](#).

Please note that technical editing may introduce minor changes to the text and/or graphics, which may alter content. The journal's standard [Terms & Conditions](#) and the [Ethical guidelines](#) still apply. In no event shall the Royal Society of Chemistry be held responsible for any errors or omissions in this *Accepted Manuscript* or any consequences arising from the use of any information it contains.

Table of Content



We summarize the state-of-the-art progress in synthesis and catalytic application of noble metal nanoparticle@metal oxide core/yolk-shell nanostructures.

Cite this: DOI: 10.1039/coxx00000x

www.rsc.org/xxxxxx

REVIEW

Noble Metal Nanoparticle@Metal Oxide Core/Yolk-Shell Nanostructures as Catalysts: Recent Progress and Perspective

Guodong Li and Zhiyong Tang*

Received (in XXX, XXX) Xth XXXXXXXXXX 20XX, Accepted Xth XXXXXXXXXX 20XX

DOI: 10.1039/b000000x

Controllable integration of noble metal (*e.g.*, Au, Ag, Pt, and Pd) and metal oxide (*e.g.*, TiO₂, CeO₂, and ZrO₂) into the single nanostructures has been attracting immense research interest in heterogeneous catalysis, because they not only combine the properties of both noble metal and metal oxide, but also bring the unique collective and synergetic functions in comparison with single-component materials. Among many strategies recently developed, one of the most efficient ways is to encapsulate and protect individual noble metal nanoparticle by a metal oxide shell of the certain thickness to generate the core-shell or yolk-shell structure, which exhibits the enhanced catalytic performance compared with conventional supported catalysts. In this review article, we summarize the state-of-the art progress in synthesis and catalytic application of noble metal nanoparticle@metal oxide core/yolk-shell nanostructures. We hope that this review will help the readers to obtain better insight into design and application of the well-defined nanocomposites in energy and environment.

1. Introduction

Catalysis is an old but evergreen field, which is now accounting for over 90% chemical processes and production of 60% chemicals worldwide.^{1, 2} In order to satisfy the urgent demand of high-performance catalysts with the characteristics of excellent activity, good selectivity and remarkable stability, catalysis, especially heterogeneous catalysis, has been undergoing comprehensive studies and innovative advances accompanied with the great progresses in nanoscience and nanotechnology over the past decade.³ Different from the conventional bulk catalysts, size shrinkage of the active components to the nanometer scale usually gives rise to significant increase in the catalytic activity due to the high surface-to-volume ratio of small particles as well as a large fraction of active atoms with dangling bonds exposed to the surface.⁴ In addition, other unique properties of nanomaterials such as surface- and strain-driven lattice distortion, variation in electronic state density and oxidation-induced charge redistribution could also benefit the catalytic performance.^{5, 6} Thanks to the rapid advances in synthesis chemistry, nanomaterials with well-defined sizes, shapes, crystal facets, structures and compositions are available,⁷⁻¹⁰ which have been providing many opportunities for developing catalysts with excellent activity for energetically challenging reactions, high selectivity to valuable products, and long-term stability under the tough reaction environment.

Among a variety of nanocatalysts developed, controllable integration of different materials such as noble metals (*e.g.*, Au, Ag, Pt, and Pd) and metal oxides (*e.g.*, TiO₂, CeO₂, and ZrO₂) into the single nanostructures has recently become one of the hottest research topics, because they not only combine the

function of individual nanoparticles (NPs), but also bring the unique collective and synergetic catalytic properties compared with single-component materials. Traditionally, these composites are easily prepared by various methods such as impregnation,^{11, 12} coprecipitation,¹³ deposition-precipitation,¹⁴ and so on. The products prepared by the conventional methods are characteristic of noble metal NPs dispersed on high-surface-area metal oxides, in which small noble metal NPs have high surface energy and tend to migrate and sinter into larger particles during the catalytic reactions, leading to loss of the unique properties registered in the original NPs.^{15, 16} To design the high-performance catalysts, many strategies have been adopted and can be generally classified into four categories: (1) Confinement of noble metal NPs into mesoporous supports,^{17, 18} (2) modification of the supports,¹⁹ (3) replacement of monocomponent noble metal NPs with alloy NPs,^{20, 21} and (4) encapsulation of noble metal NPs into the supports with the core-shell structure.²²⁻²⁶ The former three

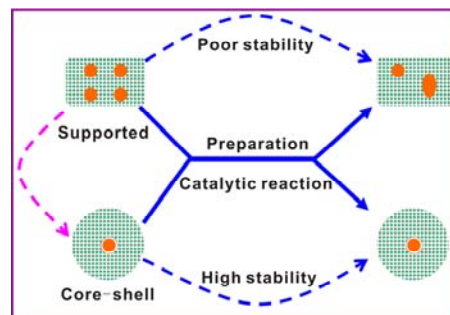


Fig. 1 Using core-shell nanostructures as an alternative of conventional supported catalysts for inhibiting the migration and aggregation of small noble metal NPs into big ones during the catalytic reaction processes.

methods may improve the catalytic performance to some extent, but cannot completely avoid migration and aggregation of noble metal NPs. As a comparison, the last one is a more effective way, because the core-shell micro-/nano-architectures have high chemical/thermal stability and recyclability (Fig. 1).

Noble metal@metal oxide core-shell nanostructures have been attracting great attention due to their unique structural features and physicochemical properties, since the pioneering work on homogeneous SiO₂ coating Au NPs was reported by Liz-Marzán *et al.*^{27, 28} Until now, a lot of work has been performed to design and construct different nanocomposites containing noble metal NP cores and metal oxide shells. Accordingly, the obtained products can be simply divided into five categories: (1) Core-shell structures refer to single noble metal core uniformly surrounded by a metal oxide shell,^{21-23, 26} (2) yolk-shell or rattle-type structures represent single movable noble metal core inside hollow metal oxide shell,²⁷ (3) sandwiched structures stand for multiple noble metal NPs as an interlayer embedded into metal oxide shell,²⁹⁻³¹ (4) multiple noble metal cores coated with metal oxide shell,³²⁻³⁶ and (5) multiple noble metal NPs embedded within metal oxide matrixes.³⁷⁻⁴³ Among the above cases,⁴⁴ individual noble metal NP is isolated in the core/yolk-shell nanostructure that enables effective inhibition of the migration and sintering of noble metal active components, suggestive of their great potential in practical applications. Moreover, in the core-shell nanostructures, the interfacial area of noble metal NP core and metal oxide shell is maximized, thus strengthening the interaction and electronic transfer between them. Meanwhile, the yolk-shell structure is characteristic of a free noble metal core inside a hollow shell with a relatively homogeneous surrounding environment, allowing for exposure of all the active sites to contact with the reactants during the catalytic process.

Based on their significance in catalysis, we intend to give a focused review of recent progress about the construction and catalytic application of noble metal NP@metal oxide core/yolk-shell nanostructures. In this review, we firstly summarize the state-of-the art progress of strategies for preparation of noble metal NP@metal oxide core/yolk-shell nanostructures with well-defined sizes, shapes and compositions. Subsequently, heterogeneous catalytic performances of these core-shell typed nanostructures in terms of activity, selectivity and stability are introduced based on a series of model reactions such as carbon monoxide oxidation, hydrogenation or selective hydrogenation, and selective oxidation. Afterwards, the relationship between the core/yolk-shell nanostructures and catalytic performances is discussed in comparison with conventional supported catalysts. Finally, we propose the emergent challenges and future developments of the core/yolk-shell structured nanocatalysts.

2. Methodologies for fabrication of noble metal NP@metal oxide core-shell nanostructures

Noble metal NP@metal oxide core-shell nanostructure is one of the simplest motifs in two-component systems, but their synthetic process is rather complex since they are susceptible to many experimental parameters including precursor, solvent, pH value, reaction temperature, reaction time, surface chemistry, and so on. Among these, the key issue involved is how to effectively

balance the heterogeneous nucleation and controllable growth of metal oxide materials onto noble metal NP surface against self-nucleation and inhomogeneous growth. Many types of noble metal NP@metal oxide core-shell nanostructures, *e.g.*, Au@TiO₂,⁴⁵⁻⁴⁷ Au@CeO₂,²² Au@Cu₂O,⁴⁸⁻⁵² Au@Fe₂O₃,⁵³ Au@Fe₃O₄,⁵⁴ Au@ZnO,⁵⁵ Au@SnO₂,^{56,57} Ag@Cu₂O,⁵⁸ Ag@CeO₂,⁵⁹ Ag@ZnO,⁶⁰ Ag@Fe₃O₄,⁶¹ Ag@SnO₂,⁶² and Pt@TiO₂,⁶³ have been successfully achieved by various strategies developed. Generally, the synthetic strategies for noble metal NP@metal core-shell nanostructures can be outlined into three groups: (1) Seeded growth based two-step method, where noble metal NPs are firstly synthesized as the seeds, followed by formation of metal oxide shells. (2) One-pot method, involving simultaneous formation of both the noble metal cores and the metal oxide shells. (3) Partial oxidation of the outside layer of noble metal NPs or selective oxidation of shell of binary metal NPs.

2.1 Seeded growth based two-step method

The Seeded growth method has been widely adopted for preparation of the core-shell nanostructures since they are straightforward to be applied and have the advantages for easily controlling the size, shape and structure of the final products. Normally, this method involves two-step process: (1) Preparation of noble metal cores with uniform sizes, shapes and structures, and (2) coating metal oxide materials onto the noble metal surfaces to form the core-shell nanostructures. So far, using noble metals as the seeds for direct metal oxide coating can be achieved via three possible modes: (1) Noble metal seed-directed epitaxial growth, (2) molecule-functionalized noble metal seeds for direct metal oxide shell coating, and (3) hydrothermal-assisted heterogeneous nucleation and growth. By tuning the experimental conditions, noble metal NP@metal oxide core-shell nanostructures with various core and shell materials have been achieved using the solution based approaches.

2.1.1 Noble metal seed-directed epitaxial growth

The prerequisite condition of the epitaxial growth method is that the lattice mismatches between different materials are less than 5%.⁶⁴ As for noble metals and metal oxides, owing to their large lattice mismatch, the obtained hybrids are usually in the form of heterodimer- or dumbbell-like nanostructures with phase separation-like growth mode, such as Au-ZnO,⁶⁵ Au-Fe₃O₄,^{66, 67} Ag-Fe₃O₄,⁶⁸ and Pt-Fe₃O₄.⁶⁹

An exceptional metal oxide is Cu₂O, which has a good chemical affinity to noble metal NPs with a relatively small lattice mismatch, preferring to form a compact and crystallized shell around noble metal NPs. As a result, many Cu₂O-based core-shell nanostructures like (Au, Ag, Pt, or Pd)@Cu₂O have been successfully synthesized.^{48, 49, 52, 58, 70, 71} For example, Huang *et al.* constructed Au@Cu₂O core-shell nanostructures by using a mixed solution containing CuCl₂, sodium dodecyl sulfate (SDS), Au NP seeds, NaOH, and NH₂OH·HCl,⁷⁰ which were added in sequence. When different-shaped Au NP cores including octahedra, highly faceted NPs, nanorods, and triangular plates were used as the seeds, the corresponding morphologies of core-shell Au@Cu₂O nanostructures were cuboctahedral, truncated stellated icosahedral, pentagonal prism and truncated triangular in turn (Fig. 2). Cross-sectional transmission electron microscopy

(TEM) and high-resolution TEM (HRTEM) images indicated that Au NP seeds guided the growth of Cu₂O shells with morphological and structural control. The (111) planes of Cu₂O were found to grow epitaxially on the {111} facets of Au NPs for most of the cases examined, while the (200) planes of Cu₂O deposited over the {200} facets of Au NPs to form the interfaces. The lattice mismatch between the (111) planes of Au and the (111) planes of Cu₂O was about 4.5%, and 4.7% between the (200) planes of Au and the (200) planes of Cu₂O. Subsequently, Mokari *et al.*⁴⁸ demonstrated that different noble metal NP@Cu₂O core-shell structures including Pt nanocubes and Pd nanocubes could be achieved, while Ag spherical plates as cores using the similar procedure was also reported by Huang *et al.*⁷⁰ It should be pointed out that there is considerably big lattice mismatch between Cu₂O and other noble metals (Pt, Pd and Ag), so the seed-directed epitaxial growth would be less expected. Fortunately, the surface reconstruction is occurred in the growth process of the Cu₂O shell, which may effectively release the interfacial stress caused by the lattice mismatch, giving rise to production of varying CuO-based core-shell nanostructures. We anticipate that this approach can be extended to preparation of other complex noble metal NP@Cu₂O structures with well-defined facets.⁵²

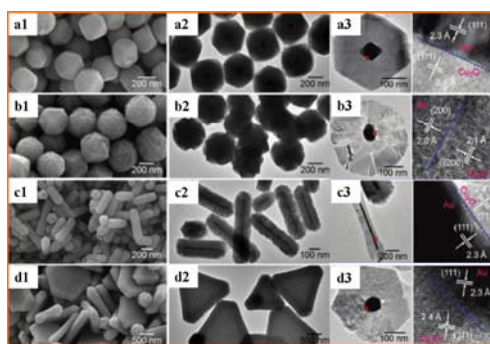


Fig. 2 Scanning electron microscopy (SEM), TEM, cross-sectional TEM and HRTEM images (red square regions) of the Au@Cu₂O core-shell nanostructures. (a1, a2, a3) Cuboctahedral heterostructures made from octahedral Au NP cores. (b1, b2, b3) Truncated stellated icosahedra formed from highly faceted Au NP cores. (c1, c2, c3) Cu₂O shells with pentagonal prism shape from 5-fold-twinned Au nanorods as templates. (d1, d2, d3) Thick truncated triangular Cu₂O plates formed from triangular and truncated triangular Au plates as templates. The Cu₂O plates are slightly concave with thinner central triangular portions. The (111) planes of Cu₂O grow epitaxially on the facets of Au, while the (200) planes of Cu₂O deposit over the {200} facets of Au to form the interfaces. Reprinted with permission from ref. 70. Copyright © 2009 American Chemical Society.

2.1.2 Molecule-functionalized noble metal seeds for directing metal oxide shell coating

As for noble metal and metal oxide of big lattice mismatches, the existence of enormous interfacial energy between them is recognized, thus resulting in difficulty for obtaining the desired core-shell products. To address these problems, the interfacial energy between the dissimilar materials should be somewhat counterbalanced by a proportional decrease in the surface energy, and therefore the requirements of lattice compatibility can be fairly less restrictive.⁷² Until now, one of the most effective ways

is to embed a layer of ligand and/or surfactant molecules between noble metal and metal oxide. Furthermore, noble metal NPs functionalized with ligand or surfactant molecules could reduce aggregation in solution via introduction of additional charge and/or steric repulsion, because the precursors for synthesizing metal oxides are usually the soluble forms of metal salts that might shield the charge repulsion among noble metal NPs to promote NP aggregation. Evidently, using suitable ligand and/or surfactant molecules is the key factor for controllable synthesis of core-shell nanostructures composed of noble metal NP core and metal oxide shell with dissimilar nature.

A plausible synthesis route is learned from the well-established recipe to prepare the noble metal NP@SiO₂ core-shell nanostructures, that is, the hydrolysis and condensation of the precursors onto the preformed noble metal NP cores such as Au@SiO₂,^{73, 74} Ag@SiO₂,⁷⁵⁻⁷⁷ Pd@SiO₂,^{45, 78} Pt@SiO₂.⁷⁹ However, different from the amorphous SiO₂ shell, the precursors used for formation of metal oxide shells possess higher reaction activity, and the metal oxide products are normally crystalline and have large the interfacial stress with noble metal cores, resulting in easy self-nucleation and uncontrollable growth of metal oxide in the solution. Therefore, it is necessary to develop powerful ligand/surfactant molecules, which can offer strong affinity to the precursors, prompt the nucleation and growth of metal oxide shells surrounding the noble metal cores. For example, Tremel *et al.* introduced oleic acid and oleylamine to synthesize flower-like Au@MnO core-shell nanostructures, in which manganese acetylacetonate (Mn(acac)₂) was decomposed in diphenyl ether in the presence of preformed Au NP cores obtained from decomposition of gold acetate (Au(OAc)₃).⁸⁰ The final products were composed of Au cores of about 7 nm in diameter and MnO petals of about 10 nm in size. This method was extended to construct Ag@MnO or Pt@MnO samples.⁸⁰ Furthermore, with the similar strategy, flower-like Au@Fe₃O₄ core-shell nanostructures with sizes of 20-28 nm are formed by using Au NPs of 7-13 nm as seeds.⁵⁴ Han *et al.* applied hydroxypropyl cellulose (0.5 wt%, Mw = 370000) to mediate TiO₂ growth to fabricate eccentric Au@TiO₂ nanostructures.⁴⁷ First, citrate-stabilized 50 nm Au NPs were modified with hydroxypropyl cellulose, and then a less reactive precursor, titanium diisopropoxide bis(acetylacetonate), was used for sol-gel coating of TiO₂ onto the Au cores. In comparison with conventional precursors such as titanium tetrabutoxide, this precursor had a much lower hydrolysis rate, which helped to separate nucleation and growth of TiO₂. Fornasiero *et al.* constructed Pd@CeO₂ core-shell nanostructures by utilizing self-assembly between the functionalized Pd NPs and cerium (IV) alkoxides.^{38, 81} The whole process mainly involved the following three parts: (1) Synthesis of thiolate-protected Pd NPs using 11-mercaptoundecanoic acid (MUA) as the passivating agent, (2) self-assembly of cerium (IV) tetrakis (decyloxyde) around Pd NPs and modification by means of dodecanoic acid, and (3) hydrolysis under controlled conditions of the remaining alkoxy groups bound to Ce atoms to obtain the dispersible Pd@CeO₂ nanostructures. Chen *et al.* developed a general synthetic methodology for coating different metal oxide shells (*e.g.*, ZnO, MnO, Fe₃O₄, Co₂O₃, TiO₂, Eu₂O₃, Tb₂O₃, and Gd₂O₃) on the citrate-stabilized noble metal seed surfaces (*e.g.*, Au, Ag, Pt and

Pd) via combination of different ligands as the intermediate agents (Fig. 3 and 4).⁵⁵ In the case of Au@ZnO core-shell nanostructures, they were achieved by using different ligand molecules including the hydrophilic thiol with –COOH end groups (e.g., 4-mercaptobenzoic acid, 2-mercaptoacetic acid, 11-mercaptoundecanoic acid) and the hydrophobic thiol-based ligands (e.g., 2-naphthalenethiol, 4-ethylthiophenol, 1-octadecanethiol, 2-dipalmitoyl-sn-glycero-3-phospho-thioethanol) in the presence of the surfactant polyvinylpyrrolidone (PVP), suggesting the generality in the use of surface ligands. In the absence of thiol ligands, only partial ZnO shells were formed on the surface of Au seeds. On the other hand, in the absence of PVP, only a thin layer of ZnO was formed on the surface of Au NPs, accompanying with additional growth and aggregation of pure ZnO NPs. When PVP was replaced by hydrophilic polyethylene-glycol (PEG), uniform ZnO shells only formed on the hydrophilic ligand-modified Au seeds, but not on the hydrophobic ones.

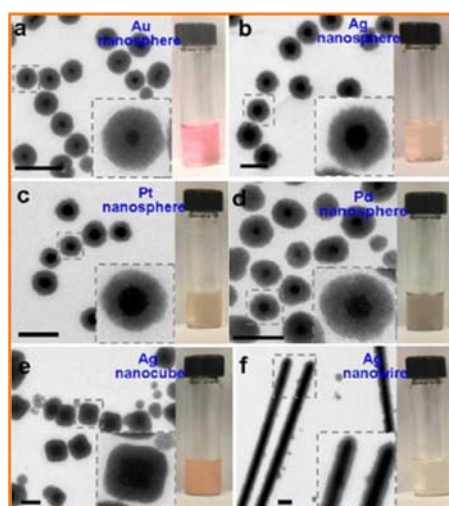


Fig. 3 TEM images and photographs of noble metal NP@ZnO core-shell structures that were synthesized from different noble metal cores: citrate-stabilized NPs, including (a) Au NPs ($d_{Au} = 15$ nm); (b) Ag NPs ($d_{Ag} = 60$ nm); and (c) Pt NPs ($d_{Pt} = 40$ nm); and PVP-stabilized NPs, including (d) Pd NPs ($d_{Pd} = 20$ nm); (e) Ag nanocubes ($d_{Ag} = 150$ nm); and (f) Ag nanowires ($d_{Ag} = 120$ nm, $l_{Ag} = 3-5$ μ m). Insets show magnified views of typical NPs. Scale bar: 200 nm. Reprinted with permission from ref. 55. Copyright © 2013 American Chemical Society.

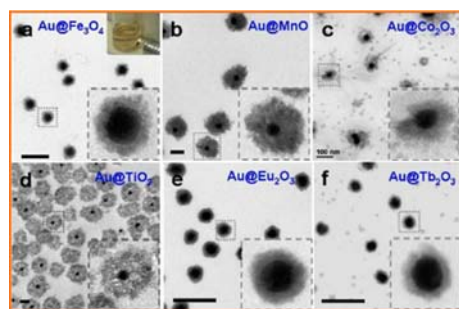


Fig. 4 TEM images of the Au@metal oxide nanostructures ($d_{Au} = 40$ nm) with different types of oxide shells: (a) Au@Fe₃O₄, (b) Au@MnO, (c) Au@Co₂O₃, (d) Au@TiO₂, (e) Au@Eu₂O₃, (f) Au@Tb₂O₃. Insets show magnified views of typical NPs. Scale bar: 200 nm. Reprinted with permission from ref. 55. Copyright © 2013 American Chemical Society.

Based on the above facts, Chen *et al.* concluded that the thiol ligand was used to modify Au surface against aggregation and reduce the Au-ZnO interfacial energy, while the surfactant PVP played multiple roles such as tuning the noble metal-ZnO interfacial energy, interfering with oxide crystal formation, and stabilizing ZnO against aggregation.⁵⁵

As introduced above, using different ligand/surfactant molecules as the intermediate agents is a simple and effective way to combine noble metals and metal oxides of different crystalline structures into the well-defined core-shell nanostructures. The generality of this strategy allows us to construct numerous noble metal NP@metal oxide core-shell nanomaterials assisted with exploration of the effective functionalized ligand/surfactant molecules.

2.1.3 Hydrothermal-assisted method

Hydrothermal method is also applied to direct metal oxide formation around noble metal seeds due to its several advantages: (1) Water is low-cost, non-toxic and environment friendly. (2) Many metal salts can be well dissolved in water as the precursors. (3) The strong polarity of water may be helpful to the controllable growth of nanocrystals.⁶⁴ Generally, the hydrothermal method is carried out in a sealed vessel, where the solvent water automatically generates the pressure upon heating and further improves the crystallinity of the prepared NPs. For example, Xu *et al.* reported a facile and green hydrothermal method to synthesize Pt@CeO₂ core-shell nanostructures, in which the citrate-stabilized Pt NPs were mixed with CeCl₃ and urea in an appropriate ratio via hydrothermal treatment at 90 °C.⁸² The obtained products were polycrystalline nature, and the diameter of Pt NP cores and the thickness of CeO₂ shells were around 100 nm and 125 nm, respectively. Chen *et al.* adopted the hydrothermal method to synthesize Au@TiO₂ core-shell

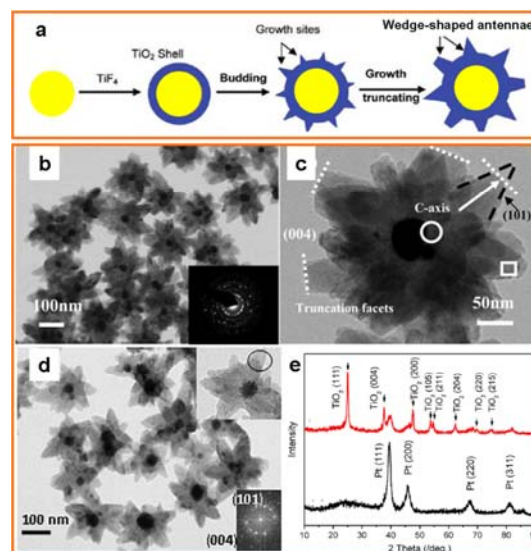


Fig. 5 (a) Scheme of the proposed formation process of core-shell Au@TiO₂ nanostructures with truncated wedge-shaped TiO₂. (b) TEM images of the prepared core-shell Au@TiO₂ and (c) individual core-shell particle image; (d) Pt@TiO₂, and (e) corresponding XRD pattern. (a-c) Reprinted with permission from ref. 83. Copyright © 2009 American Chemical Society. (d, e) Reprinted with permission from ref. 63. Copyright © 2010 Elsevier.

nanostructures with the truncated wedge-shaped TiO₂ using pre-synthesized Au NPs and TiF₄ precursors at 180 °C for 48 h (Fig. 5a).⁸² The dimension of the Au core was about 37.5 nm, and that of the wedge-like TiO₂ antennae was about 110 nm in length. The F⁻ ions not only facilitated formation of the well-defined wedge-like TiO₂ shells, but also contributed to the truncated crystal {004} facets (Fig. 5b and c).⁸³ This preparation procedure was extended successfully to synthesize other (Pd or Pt)@TiO₂ core-shell nanostructures (Fig. 5d and e),^{46, 63} indicative of general and flexible features.

In comparison with the sol-gel method, using hydrothermal method is not necessary to introduce specific ligand/surfactant molecules to facilitate the metal oxide shell formation. Obviously, hydrothermal method is simple and green, and the post treatment is more convenient. However, how to guarantee the heterogeneous nucleation and growth of metal oxides around noble metal seeds is not easily understood during the hydrothermal process, and further in-depth research work is necessary.

2.2 One-pot method

Although the two-step seed-assisted strategy can effectively isolate the preparation process of noble metal core and metal oxide shell, which enables better control over the size and structure of the products, one-pot method is still preferred in practical applications due to the reduced production cost and ease of scaling up. Using this method often involves mixing all necessary ingredients for core-shell formation in the same solution. Noble metals and metal oxides are in-situ produced simultaneously and the metal oxide shells are exclusively grown onto the surface of the noble metal NPs without self-nucleation. Therefore, accurate control over the experimental parameters including the suitable precursors, solvents, surfactants, reaction temperature, and so on are highly required to balance the nucleation and growth rates of noble metal and metal oxide and self-regulate both into single core-shell nanostructure.

To date, it still remains extremely challenging to synthesize noble metal NP@metal oxide nanostructures by using one-pot method, and the obtained synthetic methods are rather case-specific. For example, Yang *et al.* introduced a simple and convenient one-step reaction to synthesize the well-defined core-shell Ag@Fe₃O₄ nanostructures by adding octadecene (ODE) and diphenyl ether (DPE) into the mixture solution containing Ag(ac), Fe(acac)₃, 1,2-dodecanediol (DDD), oleylamine and oleic acid at 240 °C for 30 min. The obtained polycrystalline products were composed of about 6 nm Ag core and about 3 nm-thickness Fe₃O₄ shell (Fig. 6a and b).⁶⁸ The presence of the surfactants, such as oleylamine, oleic acid and DDD, was necessary for formation of Ag@Fe₃O₄ nanostructures. oleylamine and DDD as the reducing agents were responsible for the formation and stabilization of Ag cores, while oleic acid and DDD were functionalized as the surfactants for Fe₃O₄ shells. Removing any one of the surfactants from the reaction recipe would make core-shell nanostructures disappear in the product, suggesting that the synthesis was sensitive to the experimental conditions. Tang *et al.* introduced a novel one-pot hydrothermal method to fabricate the Au@CeO₂ core-shell nanostructures by using HAuCl₄, glucose, CeCl₃ and urea as raw materials.²² The formation of the

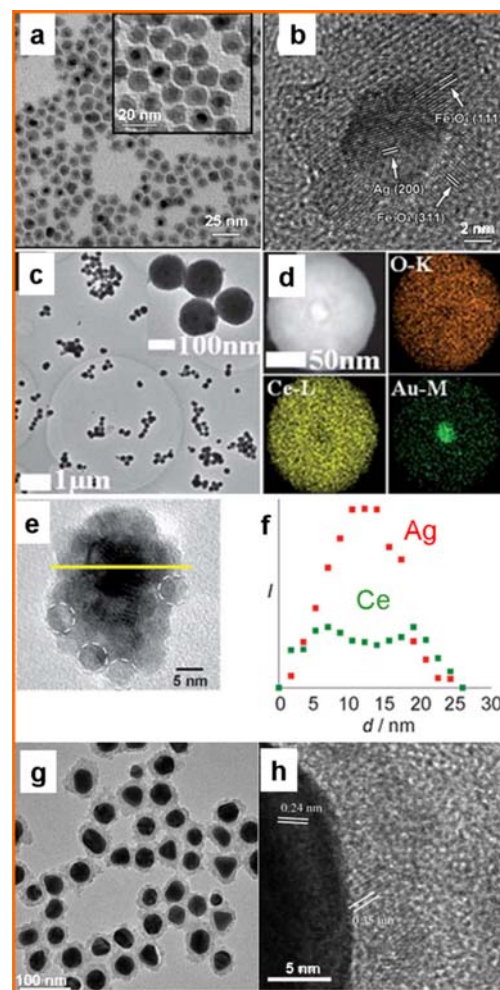


Fig. 6 TEM images of (a, b) Ag@Fe₃O₄. Reprinted with permission from ref. 68. Copyright © 2011 Royal Society of Chemistry. (c, d) Au@CeO₂. Reprinted with permission from ref. 22. Copyright © 2012 Royal Society of Chemistry. (e, f) Ag@CeO₂. Reprinted with permission from ref. 59. Copyright © 2012 Wiley-VCH. (g, h) Au@TiO₂. Reprinted with permission from ref. 45. Copyright © 2013 Royal Society of Chemistry.

Au@CeO₂ core-shell microspheres involved several steps: Firstly, reduction of Au³⁺ ions by glucose in the solution produced Au NPs. Then, condensation of glucose in solution under hydrothermal conditions led to formation of amorphous carbon microspheres, in which the Au NP was located at the center and Ce³⁺ ions were adsorbed in the matrix shell. Finally, the spontaneously formed carbon microspheres were used as the sacrificial templates to generate Au@CeO₂ microspheres through calcination in air. The obtained products were characteristic of 17 nm Au NP core surrounded by uniform CeO₂ shell composed of NPs with about 8-10 nm in diameter (Fig. 6c and d). Kaneda *et al.*^{59, 84} adopted reverse micelle technique and the redox reaction between the precursors of noble metals and metal oxides to construct Ag@CeO₂ core-shell nanostructures, where Ag NP core of about 10 nm in diameter was coated with a shell assembled by spherical CeO₂ NPs of 3-5 nm in diameter (Fig. 6e and f). Using this strategy, Au@TiO₂ core-shell nanostructures were also obtained by Dong *et al.* (Fig. 6g and h).⁴⁵ In addition, Ag@CeO₂ core-shell nanostructures were also achieved via a surfactant-free method with a subsequent

annealing redox reaction.⁸⁵ Grella *et al.* developed one-pot method to construct Ag@ZnO core-shell nanostructures by using aqueous mixture solution containing dimethylformamide (DMF), silver nitrate and zinc acetate under vigorous shaking at room temperature.⁵⁹ In this method, DMF simultaneously behaved as a reducing agent for Ag⁺ ions and provided the basic medium for zinc acetate hydrolysis without addition of any stabilizers and surfactants. The obtained products were composed of Ag core of about 20-30 nm in diameter surrounded by small ZnO units of about 10 nm in diameter.

One-pot method is relatively simple and easy to be implemented, but it is often hard to tune the sizes, shapes, compositions and uniformity of the obtained core-shell nanostructures, because of the specific experimental conditions used in a limited range for the heterogeneous nucleation and growth of metal oxides around noble metal core. Therefore, novel and effective one-pot strategies are highly desirable for synthesizing noble metal NP@metal oxide with the targeted structures.

2.3 Partial oxidation of the outermost of noble metal or selective oxidation of the shell of binary metal structures

Noble metal NP@metal oxide core-shell nanostructures can be achieved via sacrificial conversion of the outermost exposed layers of single-component NPs or selective oxidation of the metal shell of binary metal NPs. As for single-component noble metal NPs, they are possibly oxidized when exposed to air, solvated oxygen species or other oxidizing reagents, leading to formation of a metal oxide shell on the noble metal surface. However, it is rarely reported on this case due to the scarce and expensive nature of noble metals. On the contrary, as for noble metal core based binary metal NPs, the reducibility of noble metal core is much lower than that of metal shells, providing the opportunity to production of noble metal NP@metal oxide core-shell structures. For example, Xie *et al.* fabricated Au@SnO₂ core-shell particles by an intermetallics-based dry oxidation approach, in which AuSn alloy particles were subjected to a three-step oxidation process in a furnace.⁵⁷ The obtained products were composed of Au core of about 15 nm in diameter and SnO₂ shell with the thickness of 6-7 nm. Gu *et al.* prepared Pt@Fe₂O₃ core-shell nanowires by oxygen oxidation of FePt nanowires in oleylamine.⁸⁶ After oxidation, the iron in the FePt nanowires was selectively oxidized to Fe₂O₃, and the diameters were increased from 1.9 nm to 2.8 nm.⁸⁷

It should be noted that using this method, it is often difficult to control the oxidation degree of metal shell into corresponding metal oxide, thus leading to relatively poor core-shell nanostructures.

3. Methodologies for fabrication of noble metal NP@metal oxide yolk-shell nanostructures

The yolk-shell nanostructures, also called as nano-rattles, represent a special class of core-shell structures with distinctive core@void@shell configuration,⁸⁸ which has also been arousing great interest due to their complex hierarchical nanostructures and intriguing properties, such as low density, high surface area, and

interstitial hollow spaces.⁸⁹⁻⁹¹ Since the seminal work by Xia *et al.* on yolk-shell nanostructures,⁹² many research works have been developed for preparation of these structures, such as Au@TiO₂,^{93, 94} Au@ZrO₂,⁹⁵⁻⁹⁸ Au@Fe₃O₄,⁹⁹ Ag@Fe₂O₃,¹⁰⁰ Pd@CeO₂,¹⁰¹ Pt@TiO₂,¹⁰² and so on. Commonly, the synthesis methods can be simply divided into three categories: (1) Hard-templating method, (2) soft-templating method, and (3) template-free synthesis. To clearly elucidate different synthesis strategies, some examples are provided in the following.

3.1 Hard-templating method

Hard templates normally possess relatively rigid shapes, and have proved to be general and effective strategies for synthesizing movable noble metal core in a hollow metal oxide shell.¹⁰³ Typically, the synthetic procedure can be described in the following: Pre-synthesized noble metal NPs are firstly coated with a layer of hard template materials to form core-shell nanostructures, and then the target shell materials are deposited onto the surface of the template to form a sandwiched nanostructure, followed by selective removal of the template layer using dissolution with a solvent or calcination with heating. The key involved is to develop the simple and effective hard templates to bind the noble metal core and target metal oxide shell together for generating the well-defined yolk-shell nanostructures.

SiO₂ is a widely used sacrificial template to fabricate noble metal NP@metal oxide yolk-shell nanostructures.¹⁰¹ The pre-synthesized noble metal NPs were firstly coated with SiO₂ and followed by the target shell materials, producing noble metal NP@SiO₂@metal oxide three-layer "sandwich" nanostructures. Afterwards, the SiO₂ interlayer was selectively etched away with

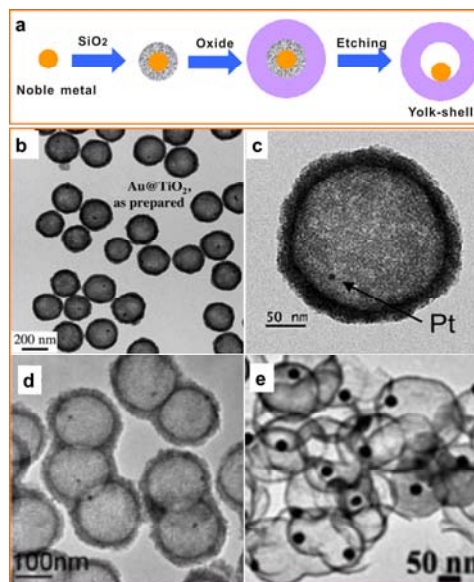


Fig. 7 (a) General scheme for synthesis of yolk-shell structures via SiO₂ template method. TEM images of (b) Au@TiO₂. Reprinted with permission from ref. 93. Copyright © 2011 Wiley-VCH. (c) Pt@TiO₂. Reprinted with permission from ref. 102. Copyright © 2012 Wiley-VCH. (d) Au@ZrO₂. Reprinted with permission from ref. 95. Copyright © 2009 Wiley-VCH. (e) Au@SnO₂. Reprinted with permission from ref. 105. Copyright © 2013 Royal Society of Chemistry.

a concentrated hydrofluoric acid¹⁰⁴ or an alkaline solution,⁹⁸ and then was subjected to calcination treatment for obtaining crystalline yolk-shell nanostructures (Fig. 7a). Despite many successful examples have been reported on preparation of Au@TiO₂ (Fig. 7b),⁹³ Pt@TiO₂ (Fig. 7c),¹⁰² Au@ZrO₂ (Fig. 7d),^{95, 97, 98} Pd@CeO₂,¹⁰¹ and Au@SnO₂ (Fig. 7e),¹⁰⁵ using SiO₂ template method is still difficult to synthesize the yolk-shell structures of the required size, shape, and surface property. For example, noble metal core or metal oxide shell is likely to be partially destroyed by the etchants accompanied with appearance of side products such as silicates^{2, 106} and titanates¹⁰⁷ and environmentally unfriendly effluent. Also, the grain sizes of metal oxide shell can fuse into large particles during high temperature calcination treatment. Furthermore, the production cost of SiO₂ template method is relatively high so that most of these methods are limited to small-scale synthesis. Therefore, to develop an alternative way to current SiO₂ template method is of great interest. Recently, Yin *et al.* reported a “surface-protected calcination” approach assisted with NaOH etching to prepare mesoporous Au@TiO₂ yolk-shell nanostructures, in which SiO₂ was used as not only a protecting agent for TiO₂ but also a hard template for hollow structures, and the corresponding intermediate configuration was described as noble metal NP@SiO₂@metal oxide@SiO₂.⁹⁴ By using different SiO₂ etching and calcination treatments, the grain sizes and crystallinity of shell materials could be effectively adjusted to some extent. Interestingly, due to the solubility of SiO₂ in hot water,¹⁰⁸ water was adopted as an alternative mild etchant to selective dissolution of SiO₂, and the obtained aqueous solution containing silica source could be recycled and reused, indicating that it will be an effective way to innovate the traditional synthesis strategy.

Selective etching of noble metal cores or metal oxide shells is another approach to synthesize noble metal NP@metal oxide yolk-shell nanostructures. Several types of yolk-shell nanostructures synthesized via the selective etching method have been reported. As an example, Schüth *et al.* employed sol-gel method to synthesize core-shell Au@SiO₂ nanostructure with big sized Au core, and then selectively etched partial Au core by KCN. Subsequently, sol-gel method was applied to coat another ZrO₂ shell onto SiO₂ surface, and finally SiO₂ template was removed to obtain Au@ZrO₂ yolk-shell nanostructures with Au core size less than 10 nm.^{97, 109} One can expect that more complex and functional yolk-shell nanostructures will be achieved by reasonable combination of different synthetic strategies together.

It should be stressed that the hard-templating methods usually require long reaction time, and it is particularly difficult to use a simple method to synthesize complex particles such as sandwich-structured particles, which are composed of noble metal cores surrounded by two different metal oxide shells (rather than one SiO₂ shell plus another metal oxide shell). Therefore, to develop the general methods to synthesize noble metal NP@metal oxide yolk-shell nanostructures, many simple and effective hard templates should be investigated in future work.

3.2 Soft-templating method

Soft templates are usually related to structure-directing molecules, such as surfactants, polymers, and even biological viruses, which are amphiphilic molecules containing a

hydrophilic head and a hydrophobic chain.¹¹⁰ These materials may spontaneously organize into well-defined assemblies under certain conditions, such as normal and reverse micelles, emulsions, vesicles, or liquid crystal phases, which geometrically restrict noble metal NPs as core and direct the growth of metal oxide around noble metal core.^{103, 110}

As an example, Li *et al.* used block copolymer as a soft template to construct Au@TiO₂ yolk-shell nanostructures.¹¹¹ Au NPs with poly(2-vinyl pyridine)-block-poly(ethylene oxide) (PVP-b-PEO) block copolymer shells were first prepared by ultraviolet (UV) irradiation of the solution of PVP-b-PEO/HAuCl₄ complexes. Then, the sol-gel reaction of titanium tetra-isopropoxide (TTIP) selectively on the surfaces of Au NPs gave rise to generation of Au-TiO₂ core-shell nanostructures. Finally, the organic interlayer inside the Au@TiO₂ core-shell nanostructures was removed by UV treatment to obtain the Au@TiO₂ yolk-shell nanostructures (Fig. 8).

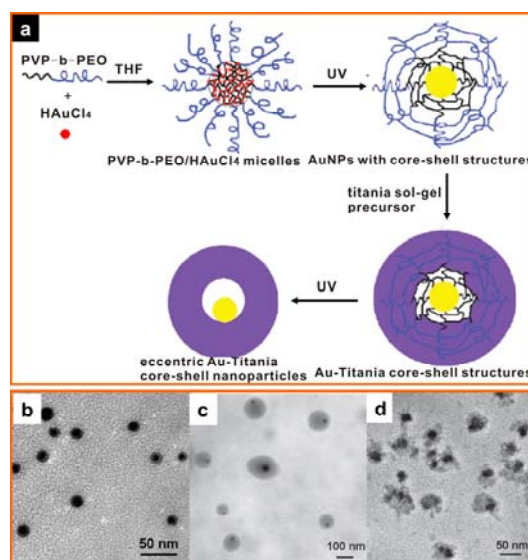


Fig. 8 (a) Schematic illustration of the process to prepare Au-TiO₂ yolk-shell nanostructures. TEM images of (b) the core-shell Au NPs prepared by irradiating a 0.05 wt% PVP-b-PEO/HAuCl₄ THF solution for 16 h, (c) core-shell Au-TiO₂ composite nanoparticles and (d) yolk-shell Au-TiO₂ NPs obtained by UV irradiation of the core-shell Au-TiO₂ nanocomposites for 4 days. Reprinted with permission from ref. 111. Copyright © 2011 Royal Society of Chemistry.

It is worth noticing that soft-templating methods often involve the complex self-assembly of structure-directing molecules and shell growth processes, and thus the soft-templating method is often limited by the difficulty in controlling the uniformity of the products and mass production.

3.3 Template-free method

Although the template-assisted methods have been proven to be very effective for synthesis of yolk-shell nanostructures, both of the hard and soft template methods have some inherent drawbacks, including low efficiency, a rather complicated and tedious process, and the difficulty in ensuring occurrence of the etching reaction exclusively inside the shells. Therefore, to develop template-free methods is important for preparation of

noble metal NP@metal oxide yolk-shell nanostructures. Generally, template-free fabrication of noble metal NP@metal oxide yolk-shell nanostructures is based on the Ostwald ripening or Kirkendall effect processes.

Ostwald ripening is driven by surface energy differences among different sized particles, and the small crystals tend to grow into those of large sizes in order to minimize their free energy.^{112, 113} This method has been employed to construct noble metal NP@metal oxide yolk-shell structures. For example, Tang *et al.* adopted an inside-out Ostwald ripening mechanism for preparation of Au@TiO₂ yolk-shell nanostructures with tunable shell thickness via hydrothermal treatment (Fig. 9).¹¹⁴ The hydrolysis of TiF₄ led to the initial formation of solid TiO₂ microspheres coating onto several small Au NPs, which gradually transformed into yolk-shell hollow spheres with a relatively large Au NP core via Ostwald ripening. The size of yolk Au core was about 10 nm, and the shell thickness could be easily adjusted from 25 nm to 150 nm by changing the amount of TiF₄ in reaction

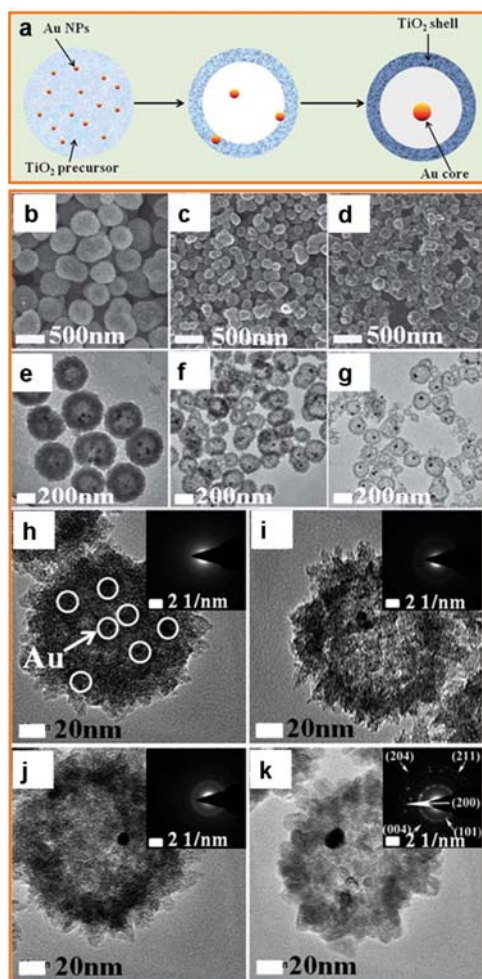


Fig. 9 (a) Scheme of formation process of Au@TiO₂ yolk-shell nanostructure via hydrothermal method. SEM of Au@TiO₂ hollow submicrospheres with (b) thick shell, (c) medium-thickness shell, and (d) thin shell. (e), (f) and (g) are corresponding TEM images of (b), (c) and (d). TEM images and SAED patterns (inset) of Au@TiO₂ yolk-shell submicrospheres with thin shell at different crystallization times: (h) 3 min, (i) 9 min, (j) 1 h and (k) 6 h. Reprinted with permission from ref. 114. Copyright © 2012 Royal Society of Chemistry.

mixture. Wang *et al.* used pre-made Au NPs as the seeds to mediate the hierarchical assembly of Cu₂O NPs in the presence of PVP (Fig. 10).⁵¹ The polycrystalline Cu₂O shells surrounding the Au cores could undergo an inside-out hollowing process driven by Ostwald ripening to form Au@Cu₂O yolk-shell nanostructures with controlled spacing between the core and the shell. Xu *et al.* developed a facile hydrothermal method to construct yolk-shell Pt@CeO₂ nanostructures using mixed aqueous solution containing Pt NPs, CeCl₃ and urea at 90 °C.⁸² By simply decreasing concentration of CeCl₃ in aqueous solution to a certain level, the initial formed core-shell Pt@CeO₂ nanostructures were transformed into yolk-shell counterparts via Ostwald ripening mechanism.

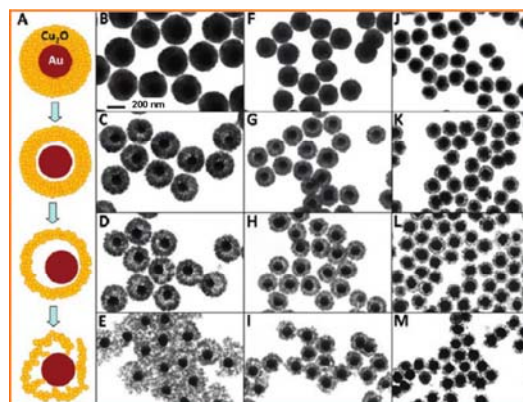


Fig. 10 Formation of Au@Cu₂O yolk-shell nanostructures. (A) Scheme of the structural evolution of Au@Cu₂O core-shell nanostructures during the hollowing of Cu₂O shell. (B-M) TEM images showing the structural evolution of Au@Cu₂O core-shell nanostructures with three different outer radii: particles with an average outer radius of 183 nm obtained at (B) 5, (C) 30, (D) 60, and (E) 90 min; particles with an average outer radius of 130 nm obtained at (F) 5, (G) 20, (H) 40, and (I) 60 min; particles with an average outer radius of 98 nm obtained at (J) 5, (K) 20, (L) 40, and (M) 60 min. All TEM images share the same scale-bar in panel B. Reprinted with permission from ref. 51. Copyright © 2011 American Chemical Society.

Kirkendall effect is referred to an atomic diffusion process that takes place via vacancy exchange rather than by direct interchange of atoms. It usually involves a fast-diffusing inner shell material to an outer layer or reservoir of a slower-diffusing material, leading to a net outward transport of matter from the inner shell and formation of voids.^{115, 116} As for the noble metal NP@metal oxide yolk-shell nanostructures, it can be achieved by transformation of core-shell binary metals via Kirkendall effect, in which the surface oxidation and vacancy diffusion selectively involves the shell portion only, while retaining the noble metal core intact. For example, Alivisatos *et al.* fabricated Au@Fe₃O₄ yolk-shell nanostructures by thermal decomposition of Fe(CO)₅ into an iron shell around the Au NPs in the presence of oleylamine and oleic acid capping molecules, and then oxidation of the iron shell into a hollow iron oxide shell by means of the Kirkendall effect.⁹⁹ The obtained products were composed of 4.5 nm yolk Au NPs with certain shell thickness by varying the molar ratio of oleylamine and oleic acid. Using this strategy, the yolk-shell Pt@Fe₂O₃,¹¹⁷ FePt@Fe₂O₃,¹¹⁷ and Ag@Fe₂O₃¹⁰⁰ NPs were also obtained.

It is noticed that template-free method is a relatively simple

and effective way to synthesize noble metal NP@metal oxide yolk-shell nanostructures. However, they require the specific properties of the target metal oxide shell material to support the formation process, which may limit its wide application in fabrication of different types of the yolk-shell nanostructures.

4. Catalytic performance of core/yolk-shell nanostructures

In comparison with the traditional supported catalysts, the core/yolk-shell noble metal NP@metal oxide nanostructures provide a great opportunity for controlling the interaction among the different components, which could boost the structural stability or catalytic activity and selectivity.^{24, 25} Though these nanostructures show many fascinating catalytic properties, the study on the catalytic performance of the core/yolk-shell nanostructures is still in its infancy, and many fundamental issues involved in the structure-reactivity relationship is still unclear. Herein, we discuss catalytic performances of these core/yolk-shell nanostructures in terms of activity, selectivity and stability based on a series of model reactions such as carbon monoxide oxidation, hydrogenation or selective hydrogenation, and selective oxidation. The relationship between the core/yolk-shell structures and catalytic performances of noble metal NP@metal oxide nanostructures is disclosed in respect with the conventional supported catalysts.

4.1 Noble metal NP@metal oxide core-shell nanostructures as catalysts

Noble metal NP@metal oxide core-shell nanostructure as the catalysts has several distinguished features compared with the traditional supported catalysts: (1) Noble metal NPs are fixed inside the metal oxide supports, and individual noble metal NP is isolated and separated by a layer of metal oxide supports, and (2) noble metal NPs are closely surrounded by metal oxide supports. These unique features may bring novel collective properties for catalytic reactions, and stimulate the extensive interest in the field of heterogeneous catalysis.

It is noticed that one of the most prominent characteristics of the core-shell nanostructures is that they can maximize the interfacial area and intensify the interaction between noble metal NPs and metal oxides, which may generate more active sites and further enhance their catalytic performance. For example, Tang *et al.* developed Au@CeO₂ core-shell nanostructures with Au core of about 17 nm in diameter for catalytic CO oxidation in comparison with the supported 14 nm Au/CeO₂ and pure CeO₂ samples (Fig. 11a).²² Impressively, Au@CeO₂ nanostructures were already active even at room temperature, and the CO conversion ratio was about 20%, whereas at this temperature, the Au/CeO₂ catalysts showed a lower conversion of 10% and pure CeO₂ submicrospheres had no activity. With increasing the reaction temperature, the complete CO conversion temperature for the Au@CeO₂ sample was about 155 °C, and as comparison the CO conversion ratios over Au/CeO₂ at 300 °C and pure CeO₂ at 310 °C were 87% and 76%, respectively. Evidently, the presence of Au NPs regardless of whether they located inside or outside the CeO₂ support could efficiently enhance the catalytic activity of CeO₂, demonstrating the synergistic effect between Au

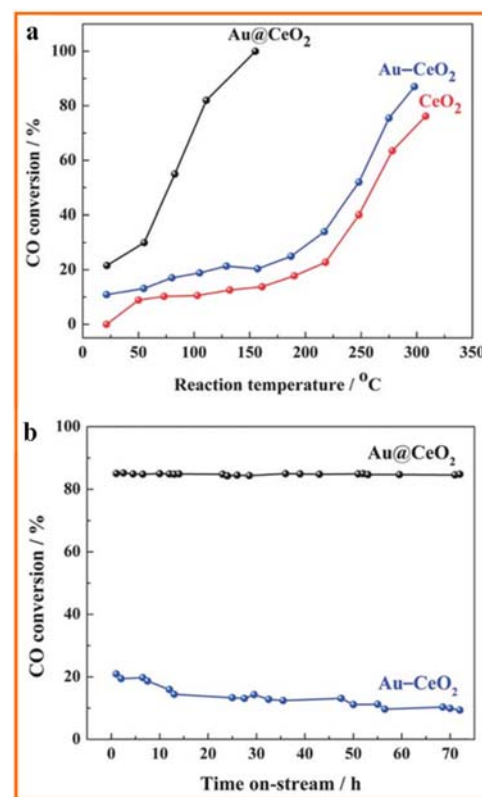
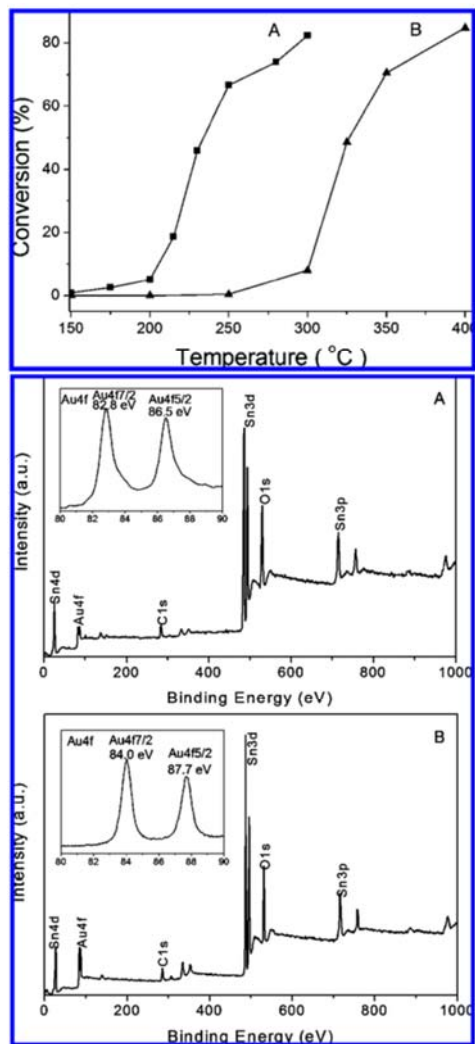


Fig. 11 (a) Catalytic activity of Au@CeO₂, Au-CeO₂, and pure CeO₂ composites for CO oxidation. Feed gas containing 1.0 vol% CO, 1.6 vol% O₂ and balance He was at a total flow rate of 50 mL min⁻¹, corresponding to a GHSV of 15000 mL h⁻¹ g⁻¹ cat. (b) Stability test of Au@CeO₂ and Au-CeO₂ at 120 °C for catalytic CO oxidation. Reprinted with permission from ref. 22. Copyright © 2012 Royal Society of Chemistry.

and CeO₂ during the catalytic process.¹¹⁸ The highest catalytic activity of the Au@CeO₂ core-shell nanostructures was attributed to the fact that the core-shell structure of Au@CeO₂ enabled maximizing the contact area between Au NP and CeO₂, while minimizing the area of bare Au NPs compared with the supported samples. Similarly, Ag@CeO₂ core-shell nanostructures with the core diameter of about 50 nm and the shell thickness of 40 nm were also used as catalysts for CO oxidation, and exhibited the enhanced catalytic performance with the low complete CO oxidation at 120 °C in respect with Ag NPs and pure CeO₂, owing to existence of strong interface interaction between the core and shell by annealing treatment.⁸⁵ Xie *et al.* studied the Au@SnO₂ core-shell nanostructures containing 15 nm Au cores and 6-7 nm SnO₂ shell for catalytic CO oxidation in comparison with the supported Au/SnO₂ samples (Fig. 12).⁵⁷ The half conversion temperature for Au@SnO₂ samples was about 230 °C, while it was 330 °C for the supported Au/SnO₂. Notably, the supported Au/SnO₂ catalyst was observed to suffer a substantial loss in the activity compared to the core-shell Au@SnO₂. To verify the synergistic effect between Au and SnO₂, X-ray photoelectron spectroscopy (XPS) survey was performed, and the result indicated that the lowest Au 4f_{7/2} electron binding energy (BE) level was located at 82.8 eV for the core-shell Au@SnO₂, implying that Au in the Au@SnO₂ core-shell structure was in a metallic state. Interestingly, the Au 4f_{7/2} spectrum showed a negative BE shift of -1.3 eV with respect to that of metallic Au

(84.1 eV) inside the supported Au/SnO₂ samples. The shift of Au 4f binding energy might be ascribed to two possible factors: (1) Small sizes of Au NPs, and (2) electronic transfer from oxide support to the Au NPs.¹¹⁸ In this study, since the size of Au NPs was relatively big, such negative BE shift should be caused by the strong interactions between Au and SnO₂ in the core-shell structure, resulting in enhancement of its catalytic performance for CO oxidation.



10

Fig. 12 Catalytic performance of (A) Au@SnO₂ and (B) supported Au/SnO₂ for CO oxidation. The reaction gas, a mixture composition of 10% CO in air, was fed to a 50 mg catalyst at a rate of 70 mL min⁻¹, which corresponded to a space velocity of 84000 cm³ h⁻¹ g_{cat}⁻¹. Reprinted with permission from ref. 57. Copyright © 2008 American Chemical Society.

Very intriguingly, the functionality synergy between noble metal core and metal oxide shell can not only maximize the number of desirable active sites at the interface of the catalyst, but also minimize the presence of other sites that may promote undesirable side reactions. For example, Kaneda *et al.* investigated Ag@CeO₂ core-shell nanostructures with 10 nm Ag core and a shell assembled with spherical CeO₂ NPs of 3-5 nm in diameter for chemoselective hydrogenation. It was found that the nano-gaps among the adjacent CeO₂ NPs in the shell permitted

25

the access of reactants to the active Ag sites in the core.^{59, 84} Maximizing the interaction between Ag NPs and the basic sites of CeO₂ successfully induced the heterolytic cleavage of H₂ to Ag-hydride and proton species rather than homolytic cleavage of H₂ on the bare Ag surface of the supported Ag/CeO₂ samples (Fig. 13a). Correspondingly, the core-shell nanostructures exhibited the excellent chemoselective reduction of nitrostyrenes, epoxides and unsaturated aldehydes, while maintaining the C=C bonds. For instance, the core-shell nanostructures had high chemoselective conversion (> 99%) of 3-nitrostyrene to 3-aminostyrene under high pressure H₂ at 110 °C (Fig. 13b and c), the excellent activity (98%) and selectivity (>99%) for the catalytic deoxygenation of epoxides to alkenes, and the enhanced chemoselective reduction (>99%) of unsaturated aldehydes to the corresponding allylic

40

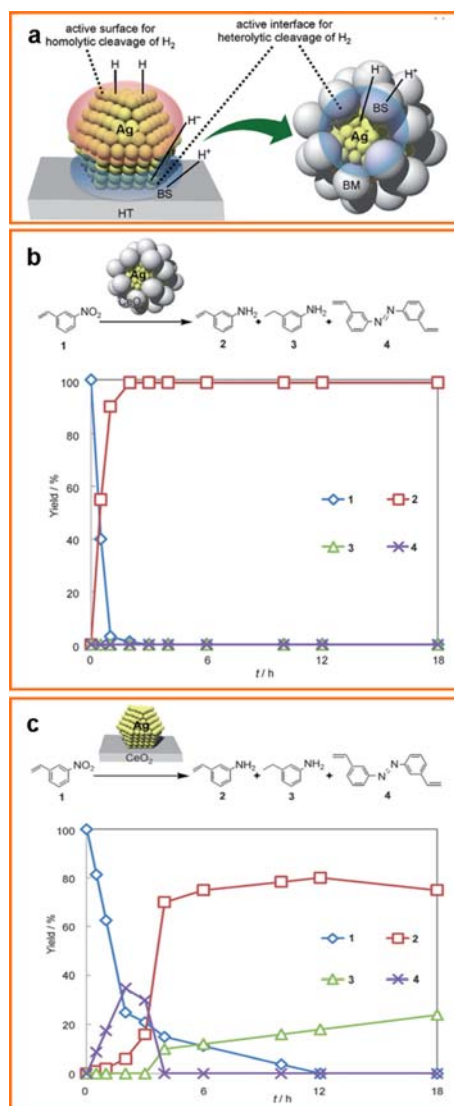
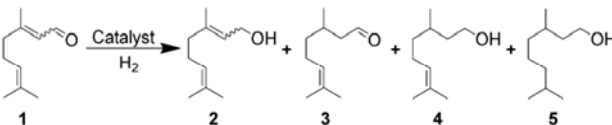


Fig. 13 (a) Catalyst design of core-shell nanocomposite for chemoselective reductions with H₂. Representation of Ag/HT reacting with H₂; both polar and nonpolar hydrogen species were formed. Ag NPs were covered with a basic material (BM), which react with H₂ to result in the exclusive formation of polar hydrogen species. A basic site of HT and BM was represented by BS. Time course of the reduction of nitrostyrene with H₂ using (b) Ag@CeO₂ and (c) Ag/CeO₂. Reprinted with permission from ref. 59. Copyright © 2012 Wiley-VCH.

alcohols (Table 1). Furthermore, Ag@CeO₂ could be highly dispersed on the CeO₂ matrix, exhibiting six times higher catalytic activity than the original Ag@CeO₂ as well as a wide applicability for various substrates in the chemoselective reductions of unsaturated aldehydes. Gu *et al.* studied Pt@Fe₂O₃ nanowires with a diameter of 2.8 nm as catalysts for selective oxidation of styrene, and these core-shell nanowires showed much higher activity than pure Fe₂O₃ and Pt@Fe₂O₃ hollow NPs, with a yield of benzaldehyde of 31.3% (Table 2 and Fig. 14).⁸⁶

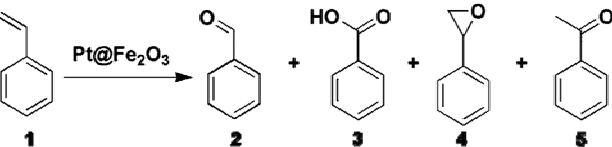
Table 1 Reduction of citral using various catalysts.^[a] Reprinted with permission from ref. 84. Copyright © 2013 Wiley-VCH.



Catalyst	t (h)	Conv. (%) ^[b]					Sel. (%) ^[b]				
		1	2	3	4	5	1	2	3	4	5
Ag@CeO ₂ (Ag/Ce=1.5)	72	>99	96	1	3	0					
Ag@CeO ₂ (Ag/Ce=0.5)	72	21	>99	<1	<1	0					
Ag@CeO ₂ (Ag/Ce=2.5)	72	92	88	2	10	0					
Ag/CeO ₂	72	97	86	3	11	0					
Ag NPs	12	4	0	0	0	0					
CeO ₂	12	3	0	0	0	0					

[a] Reaction conditions: Catalyst (metal: 0.008 mmol), substrate (0.25 mmol), THF (5 mL), 150 °C, H₂ (15 atm). [b] Determined by GC using an internal standard.

Table 2 Optimisation of the reaction conditions for the selective oxidation of styrene with a Pt@Fe₂O₃ nanowire catalyst.^[a] Reprinted with permission from ref. 86. Copyright © 2011 Wiley-VCH.



Solvent	Oxidation	T (°C)	Conv. (%) ^[b]					Sel. (%) ^[b]				
			1	2	3	4	5	1	2	3	4	5
DMF	O ₂	60	45.2	49.3	19.7	30.9	0.1					
acetonitrile	O ₂	60	43.5	71.9	4.5	23.6	NA					
dioxane	O ₂	60	38.7	74.4	3.7	21.9	NA					
DMSO	O ₂	60	37.7	80.6	2.8	16.6	NA					
CHCl ₃	O ₂	60	35.9	58.2	14.0	27.6	0.2					
Toluene	O ₂	60	22.3	90.0	1.2	8.4	0.4					
THF	O ₂	60	18.2	81.4	3.7	14.9	NA					
Water	O ₂	60	10.1	91.0	0.2	8.8	NA					

[a] Reagents and conditions: 0.8 mg Pt@Fe₂O₃ nanowires (25 wt.% Fe₂O₃ in the Pt@Fe₂O₃ nanowires), 4.5 mmol styrene, 2 mL solvent, 24 h, 1 atm oxygen. [b] Calculated by GC-MS using tert-butylbenzene as an internal standard.

The interface between Pt and Fe₂O₃ was identified as the active centre for activation of O₂.¹¹⁹ This interface activation effect was further confirmed by the catalytic performances of Pt@Fe₂O₃ yolk-shell NPs (Fig. 14, column 4) and Pt@Fe₂O₃ nanowires (Fig. 14, column 1). The yolk-shell NPs had no Pt-Fe₂O₃ interface and thus a low conversion of styrene was observed. Evidently, the synergistic effect between noble metal NPs and catalytic active metal oxides brought a positive promotion to the target products, and the active sites for these reactions should mainly lie in the interface of both rather than single components.

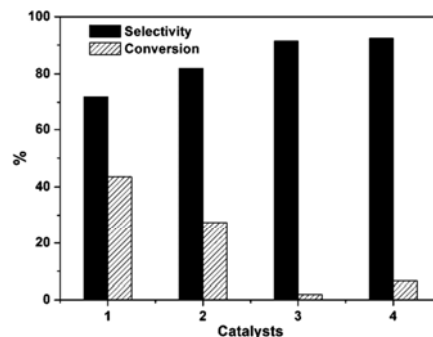


Fig. 14 Catalytic performance of Pt@Fe₂O₃ nanowires in the conversion of styrene and benzaldehyde selectivity compared with other catalysts. 1) Pt@Fe₂O₃ nanowires, 2) Fe₂O₃ NPs, 3) FePt NPs and 4) Pt@Fe₂O₃ yolk-shell NPs. Reprinted with permission from ref. 86. Copyright © 2011 Wiley-VCH.

It should be pointed out that until now, the functionality synergy between noble metal and metal oxide is only focused on a certain type of reactions, but not on all the catalytic reactions. For example, Au and TiO₂ are both active for catalytic oxidation and photocatalytic reactions,^{120, 121} and supposed to exhibit the enhanced catalytic performance when integrated into single nanostructure. However, when the Au@TiO₂ core-shell nanostructures with 40 nm Au core and TiO₂ shell of 5 nm in thickness were used as catalysts for reduction of 4-nitrophenol by NaBH₄, they showed relatively lower activity than the supported 50 nm Au/TiO₂. The control experiments indicated that bare TiO₂ did not possess catalytic activity towards the reduction of 4-nitrophenol.⁴⁵ This result suggested that the outer TiO₂ shell in the core-shell nanostructures inevitably blocked a certain amount of the active surface of noble metal cores, thus leading to the partial loss in the activity of original noble metal NPs. Doong *et al.* evaluated the flower-like Au@Fe₃O₄ core-shell nanostructures with core diameters of about 7-13 nm and shell thickness of about 20-28 nm as catalysts for reduction of 4-nitrophenol and 2,4-dinitrophenol by NaBH₄ in comparison with dumbbell-like structures.⁵⁴ The rate constants were 0.38 min⁻¹ for 4-nitrophenol and 0.46 min⁻¹ for 2,4-dinitrophenol by using the Au@Fe₃O₄ core-shell nanostructures, whereas using the dumbbell-like structures, they were 0.63 min⁻¹ and 0.72 min⁻¹ for 4-nitrophenol and 2,4-dinitrophenol, respectively. The catalytic performance of the flower-like Au@Fe₃O₄ was lower than that of the dumbbell-like structures, disclosing the fact that the Au surfaces in the flower-like structures were mainly occupied by the Fe₃O₄ shells and thus the reduction rate of nitrophenols was suppressed. Therefore, it is of great importance to design the nanocatalysts of rational structures and compositions for the specific type of

reactions.

Besides the catalytic activity and selectivity, chemical or thermal stability is another important parameter to evaluate the performance of a catalyst. Since individual noble metal NP is isolated and separated by metal oxide supports, the core-shell nanostructures are expected to display better stability in comparison with the traditional supported catalysts. Tang *et al.* evaluated the stability of Au@CeO₂ as catalysts for catalytic CO oxidation in comparison with supported Au/CeO₂ samples (Fig. 11b).²² At 120 °C, the CO conversion ratio was around 85.1% and 20.9% on the Au@CeO₂ and Au/CeO₂ catalysts, respectively. When the catalytic reaction was performed at 120 °C for 72 h, no deactivation occurred for the Au@CeO₂ core-shell submicrospheres. The TEM image further demonstrated that there were no obvious changes in the size, shape and structure of the core-shell submicrospheres. In contrast, the deactivation happened over the Au/CeO₂ catalyst, and the corresponding CO conversion ratio at 120 °C was decreased from 20.9% to 9.3% after 72 h reaction. In this work, the deactivation was mainly caused by migration and sintering of Au NPs in the supported Au/CeO₂ catalysts, which was proved by TEM observation that the average sizes of Au NPs were increased from original 14 nm to 18 nm after the catalytic reaction.

Though the core-shell structured catalysts exhibit many advantages in heterogeneous catalysis in comparison with the supported samples, there also exist some disadvantages for catalytic reactions. For instance, the diffusion rates of both the reactants and the products toward the noble metal NP cores are significantly reduced, especially for the liquid-phase catalytic reactions, since they are deeply buried in the support matrix. Therefore, it is imperative to fabricate the core-shell nanostructures with specific sizes, shapes, structures, channels and compositions as well as understand the relationship between the core-shell structure and their catalytic performance, in order to improve the performance for different catalytic reactions.

4.2 Noble metal NP@metal oxide yolk-shell nanostructures as catalysts

Analogously to the core-shell nanostructures, the yolk-shell nanostructures can also stabilize the active noble metal cores and prevent leaching or particle agglomeration, thus endowing the excellent catalytic stability.^{93, 101} Furthermore, the yolk-shell nanostructures as nanoreactors have their unique features for catalytic reactions: (1) Free noble metal core is located inside a hollow shell with a relatively homogeneous surrounding environment, thus sufficiently exposing their active sites to contact with the reactants during the catalytic process. (2) Strong interactions between noble metal core and catalytic active metal oxide shell are maintained via physical or chemical contacts in the structure. (3) The interstitial hollow space can allow high loading of guest molecules, such as the reactants for catalysis. Such characteristics may bring novel properties and offer wide applications in heterogeneous catalysis.

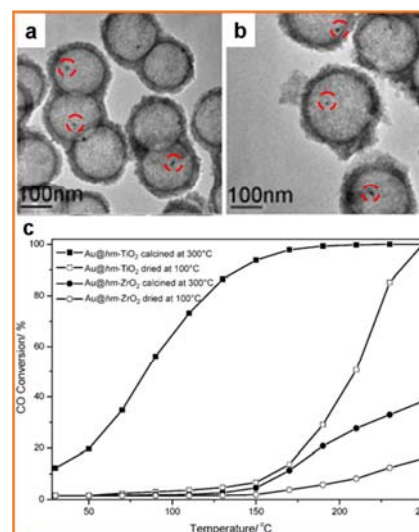


Fig. 15 TEM images of (a) Au@ZrO₂, (b) Au@TiO₂ yolk-shell nanostructure (red circles stand for Au NPs). (c) A comparison of catalytic activity in CO oxidation by Au@TiO₂ and Au@ZrO₂ yolk-shell nanostructures treated at 100 °C and 300 °C. Catalytic conditions: 50 mg catalyst, 50 mL 1% CO balanced with air. Reprinted with permission from ref. 95. Copyright © 2009 Wiley-VCH.

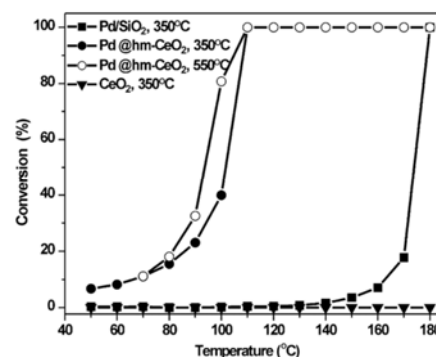


Fig. 16 CO oxidation conversion curves of the Pd@CeO₂ yolk-shell catalyst treated at 350 °C and 550 °C, supported Pd/SiO₂ NPs calcined at 350 °C, and hollow CeO₂ treated at 350 °C. Reprinted with permission from ref. 101. Copyright © 2012 Wiley-VCH.

Schüth *et al.* investigated the catalytic activity of Au@ZrO₂ yolk-shell nanostructures with a Au core of about 14 nm for CO oxidation in comparison with Au@C yolk-shell nanostructures of the same core size.⁹⁶ The activity of carbon-based catalysts was at least one order of magnitude lower than that of ZrO₂-based systems, indicating that ZrO₂ had strong positive effect on the activity of Au NPs. Stucky *et al.* studied the Au@ZrO₂ yolk-shell nanostructures with 6.3 nm Au core and 20 nm ZrO₂ shell for catalytic CO oxidation (Fig. 15),⁹⁵ and found no significant activity even after treatment at 300 °C. As comparison, the yolk-shell nanostructures with TiO₂ shells exhibited better performance, especially after being calcined at 300 °C, revealing better synergistic effect between Au NP core and the porous TiO₂ shell. Zheng *et al.* used the multi-yolk-shell Pd@CeO₂ nanocatalysts with 5 nm yolk Pd cores for catalytic CO oxidation (Fig. 16).¹⁰¹ These nanocomposites displayed a high catalytic activity with 100% CO conversion at 110 °C. To further explore the role of CeO₂ shells during catalytic CO oxidation, the

supported Pd/SiO₂ samples were used as the contrast samples, which showed the complete oxidation of CO at temperatures of above 180 °C. This result demonstrated a significant promotion effect of CeO₂ on the catalytic activity of the Pd NPs in the yolk-shell nanostructures.

Impressively, both the movable core and hollow shell in the yolk-shell nanostructure are easily tailored and functionalized to generate novel properties, and the enclosed void space of yolk-shell nanostructures could be used for confinement of more reactants accessible to noble metal cores. For example, Schüth *et al.* synthesized Au@ZrO₂ yolk-shell nanostructures with 15 nm Au cores for catalytic CO oxidation (Fig. 17).¹²² It was found that the temperature for complete conversion was about 200 °C. A further enhancement in the activity was achieved by simply doping these materials with small amounts of TiO₂ around the yolk Au NPs.

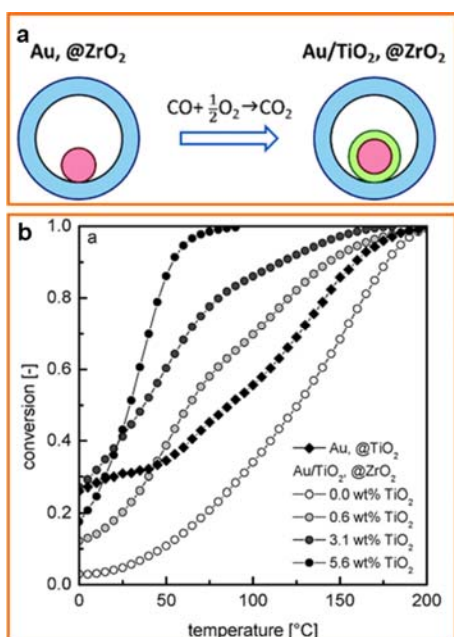


Fig. 17 (a) Scheme of Au@ZrO₂ and Au/TiO₂, @ZrO₂ yolk-shell nanostructure, and (b) their catalytic performance for CO oxidation in comparison with Au@TiO₂. Reprinted with permission from ref. 122. Copyright©2011 Royal Society of Chemistry.

5. Conclusion and outlook

We have reviewed the recent progress in construction of noble metal NP@metal oxide core/yolk-shell nanostructures as well as their applications in heterogeneous catalysis. With the rapid development of synthesis chemistry, many noble metal NP@metal oxide core/yolk-shell nanostructures have been successfully fabricated via different strategies, *e.g.*, seed-based two-step growth, one-pot method and partial oxidation of the outer-layer metals for the core-shell nanostructures; template-assisted method and template-free method for the yolk-shell nanostructures. Remarkably, when both nanostructures are used as catalysts, they have exhibited many unique advantages as follows: (1) The metal oxide shells effectively encapsulate the

active noble metal cores and prevent leaching or severe particle agglomeration in comparison with the traditional supported catalysts, thus exhibiting the enhanced chemical or thermal stability during the catalytic process. (2) The maximized contacting interface between noble metal cores and metal oxide shells in the core-shell nanostructures could bring new possibilities for generating the collective properties and tuning the catalytic functions. (3) Free noble metal cores inside the hollow shells allow for exposure of their whole surface to contact with the reactants in a relatively homogeneous surrounding environment, which result in increase of the reaction rates. (4) The metal oxide shells in the core/yolk-shell nanostructures are easily tailored to offer a number of functionalities, for instance, selective percolation of molecules in and out to improve the catalytic selectivity.

However, though tremendous advances have been made, the study on core/yolk-shell nanostructures is still in its infancy, and many challenges remain to be solved: (1) Most synthetic strategies described the above are in general not viable for synthesis of noble metal cores with the sizes of less than 10 nm, which is considerably bigger than the critical size to achieve the high catalytic performance. For example, Au NPs of 2-5 nm in size that are supported on transition metal oxides such as Fe₂O₃,¹²³ TiO₂,¹²⁴ and ZnO¹²⁵ have been found to exhibit the exceptional catalytic activity for CO oxidation at room temperature or lower. Furthermore, shape selectivity is one of the crown jewels in heterogeneous catalysis,³³ and different shapes of core-shell nanostructures are highly correlated with their catalytic properties; however, the morphology control of both the cores and the shells are rarely reported. (2) Though different strategies have been developed to fabricate the core/yolk-shell nanostructures, most of the obtained shell materials are limited to several metal oxides, such as TiO₂, CeO₂, and ZrO₂. As a result, the core/yolk-shell nanocomposites possess the limited capacity to tailor the catalytic properties of the core-shell nanostructures. (3) In most of the core/yolk-shell catalysts, the metal oxide shell are typically served with only one function, that is, acting as a protective layer to prevent aggregation between particles during the reaction. As a result, previous works are mainly focused on investigation of single-step reaction, and the multi-step cascade reactions via both shells and cores are rarely reported, which are extremely important for sustainable synthesis with lower cost, fewer chemicals and less energy. (4) In comparison with traditional supported catalysts, the unique collective and synergetic functions of noble metal core and metal oxide shell in the core/yolk-shell nanostructures are still not well understood, mainly due to the difficulty in precise control of the surface structure of noble metal cores, the diffusion rates of reactants through porous metal oxide shell, and the limited characterization on the interface between cores and shells. Therefore, the knowledge on correlations between the physiochemical properties and the catalytic performance of the core/yolk-shell nanostructures is preliminary.

To solve the above challenges, herein we suggest the on-going research works for the core/yolk-shell nanostructures as catalysts: (1) It is extremely important to develop new synthetic methods or modify current techniques to construct the well-defined noble metal NP@metal oxide core/yolk-shell nanostructures, in which

the sizes and shapes of noble metal cores as well as the thicknesses and structures of the metal oxide shells can be tuned. More importantly, the mechanism about the heterogeneous nucleation and growth of the metal oxide shells on the surface of noble metal cores need to be studied in detail, and the interfacial transition between the cores and the shells should be further illustrated. (2) More functionality should be explored for the core/yolk-shell nanostructures in order to target different catalytic reactions. The design and creation of more complex core/yolk-shell structures with multiple components and well-controlled interactions are required to upgrade the simplest motif in two-component systems, such as noble metal cores in the form of alloy or core-shell structure,¹²⁶⁻¹²⁸ composite metal oxides as the shell materials,¹²⁹ or combination of both. Such core/yolk-shell nanostructures of the complex arrangements are likely to bring new benefits to many one-step catalytic reactions and even to multiple cascade reactions. (3) Armed with different characterization techniques and theory calculations, the fundamental understanding is highly desirable to better tune the catalytic performance of the core/yolk-shell nanostructure, e.g., the diffusion and transfer behaviours of both reactants and products via the shells, the charge distribution between the shells and cores, the Schottky barrier at the interface between metal oxide and noble metal, and *etc.* To identify these knowledges will contribute to fabrication of the core/yolk-shell nanostructures with high activity, excellent selectivity and long-term stability.

In conclusion, as the alternatives of the traditional supported catalysts, noble metal NP@metal oxide core/yolk-shell nanostructures have been showing great potential as a new generation of high-performance catalysts, which will eventually benefit the sustainable industrial applications in the future.

Acknowledgements

This work was supported financially by National Research Fund for Fundamental Key Project (2014CB931801, Z.Y.T.), National Natural Science Foundation for Distinguished Youth Scholars of China (21025310, Z.Y.T.), National Natural Science Foundation of China (91027011, Z.Y.T.; 21303029, G.D.L.).

Notes and references

Laboratory for Nanomaterials, National Center for Nanoscience and Technology, Beijing, 100190, P. R. China, Fax: (+86) 010-62656765; E-mail: zytang@nanoctr.cn

† Electronic Supplementary Information (ESI) available: [details of any supplementary information available should be included here]. See DOI: 10.1039/b000000x/

‡ Footnotes should appear here. These might include comments relevant to but not central to the matter under discussion, limited experimental and spectral data, and crystallographic data.

- C.-J. Zhong and M. M. Maye, *Adv. Mater.*, 2001, **13**, 1507.
- F. Zaera, *J. Phys. Chem. Lett.*, 2010, **1**, 621.
- I. Lee, M. A. Albiter, Q. Zhang, J. Ge, Y. Yin and F. Zaera, *Phys. Chem. Chem. Phys.*, 2011, **13**, 2449.
- H. Goesmann and C. Feldmann, *Angew. Chem. Int. Ed.*, 2010, **49**, 1362.
- M. Chiesa, M. C. Paganini, E. Giamello, D. M. Murphy, C. D. Valentin and G. Pacchioni, *Acc. Chem. Res.*, 2006, **39**, 861.
- J. Zhao, B. Li, K. Onda, M. Feng and H. Petek, *Chem. Rev.*, 2006, **106**, 4402.
- A. Roucoux, J. Schulz and H. Patin, *Chem. Rev.*, 2002, **102**, 3757.

- Y. Sun and Y. Xia, *Science*, 2002, **298**, 2176.
- A. R. Tao, S. Habas and P. Yang, *Small*, 2008, **4**, 310.
- C.-Y. Chiu, P.-J. Chung, K.-U. Lao, C.-W. Liao and M. H. Huang, *J. Phys. Chem. C*, 2012, **116**, 23757.
- S.-H. Oh and G. B. Hoflund, *J. Phys. Chem. A*, 2006, **110**, 7609.
- K. Zorn, S. Giorgio, E. Halwax, C. R. Henry, H. Grönbeck and G. Rupprechter, *J. Phys. Chem. C*, 2011, **115**, 1103.
- J. Guzman, S. Carretin, J. C. Fierro-Gonzalez, Y. Hao, B. C. Gates and A. Corma, *Angew. Chem. Int. Ed.*, 2005, **44**, 4778.
- Y. Wang, S. Van de Vyver, K. K. Sharma and Y. Román-Leshkov, *Green Chem.*, 2013, doi: 10.1039/c3gc41362d.
- A. Corma and H. Garcia, *Chem. Soc. Rev.*, 2008, **37**, 2096.
- A. Cao, R. Lu and G. Veser, *Phys. Chem. Chem. Phys.*, 2010, **12**, 13499.
- C. Chen, C. Nan, D. Wang, Q. Su, H. Duan, X. Liu, L. Zhang, D. Chu, W. Song, Q. Peng and Y. Li, *Angew. Chem. Int. Ed.*, 2011, **50**, 3725.
- C. Y. Ma, Z. Mu, J. J. Li, Y. G. Jin, J. Cheng, G. Q. Lu, Z. P. Hao and S. Z. Qiao, *J. Am. Chem. Soc.*, 2010, **132**, 2608.
- K. Zhao, B. Qiao, J. Wang, Y. Zhang and T. Zhang, *Chem. Commun.*, 2011, **47**, 1779.
- X. Liu, A. Wang, X. Wang, C.-Y. Mou and T. Zhang, *Chem. Commun.*, 2008, 3187.
- J. Feng, C. Ma, P. J. Miedziak, J. K. Edwards, G. L. Brett, D. Li, Y. Du, D. J. Morgan and G. J. Hutchings, *Dalton Trans.*, 2013, **42**, 14498.
- J. Qi, J. Chen, G. Li, S. Li, Y. Gao and Z. Tang, *Energy Environ. Sci.*, 2012, **5**, 8937.
- R. G. Chaudhuri and S. Paria, *Chem. Rev.*, 2012, **112**, 2373.
- Q. Zhang, I. Lee, J. B. Joo, F. Zaera and Y. Yin, *Acc. Chem. Res.*, 2013, **46**, 1816.
- H. C. ZENG, *Acc. Chem. Res.*, 2013, **46**, 226.
- S. Liu, S.-Q. Bai, Y. Zheng, K. W. Shah and M.-Y. Han, *ChemCatChem*, 2012, **4**, 1462.
- L. M. Liz-Marzán and A. P. Philipse, *J. Colloid Interf. Sci.*, 1995, **176**, 459.
- L. M. Liz-Marzán, M. Giersig and P. Mulvaney, *Langmuir*, 1996, **12**, 4329.
- Y. Dai, B. Lim, Y. Yang, C. M. Cobley, W. Li, E. C. Cho, B. Grayson, P. T. Fanson, C. T. Campbell, Y. Sun and Y. Xia, *Angew. Chem. Int. Ed.*, 2010, **49**, 8165.
- Q. Zhang, D. Q. Lima, I. Lee, F. Zaera, M. Chi and Y. Yin, *Angew. Chem. Int. Ed.*, 2011, **50**, 7088.
- H. -S. Wu, L. -D. Sun, H. -P. Zhou and C. -H. Yan, *Nanoscale*, 2012, **4**, 3242.
- N. Zhang and Y. -J. Xu, *Chem. Mater.*, 2013, **25**, 1979.
- Z. Chen, Z.-M. Cui, P. Li, C.-Y. Cao, Y.-L. Hong, Z.-y. Wu and W.-G. Song, *J. Phys. Chem. C*, 2012, **116**, 14986.
- K.-T. Li, M.-H. Hsu and I. Wang, *Catal. Commun.*, 2008, **9**, 2257.
- Z. Chen, Z. -M. Cui, F. Niu, L. Jiang and W. -G. Song, *Chem. Commun.*, 2010, **46**, 6524.
- N. Zhang, S. Liu, X. Fu and Y.-J. Xu, *J. Phys. Chem. C*, 2011, **115**, 22901.
- H. -L. Jiang, T. Umegaki, T. Akita, X. -B. Zhang, M. Haruta and Q. Xu, *Chem. -Eur. J.*, 2010, **16**, 3132.
- L. D. Rogatis, M. Cargnello, V. Gombac, B. Lorenzut, T. Montini and P. Fornasiero, *ChemSusChem*, 2010, **3**, 24.
- M. Cargnello, T. Montini, S. Polizzi, N. L. Wieder, R. J. Gorte, M. Graziani and P. Fornasiero, *Dalton Trans.*, 2010, **39**, 2122.
- L. Kong, G. Duan, G. Zuo, W. Cai and Z. Cheng, *Mater. Chem. Phys.*, 2010, **123**, 421.
- M. Cargnello, C. Gentilini, T. Montini, E. Fonda, S. Mehraeen, M. Chi, M. Herrera-Collado, N. D. Browning, S. Polizzi, L. Pasquato and P. Fornasiero, *Chem. Mater.*, 2010, **22**, 4335.
- Y. Yu, C. Y. Cao, Z. Chen, H. Liu, P. Li, Z. F. Dou and W. G. Song, *Chem. Commun.*, 2013, **49**, 3116.
- M. -H. Jung, Y. J. Yun, M. -J. Chu and M. G. Kang, *Chem. -Eur. J.*, 2013, **19**, 8543.
- Z. Ma and S. Dai, *ACS Catal.*, 2011, **1**, 805.
- L. Han, C. Zhu, P. Hu and S. Dong, *RSC Adv.*, 2013, **3**, 12568.

- 46 N. Zhang, S. Liu, X. Fu and Y.-J. Xu, *J. Phys. Chem. C*, 2011, **115**, 9136.
- 47 Z. W. Seh, S. Liu, S. -Y. Zhang, K. W. Shah and M. -Y. Han, *Chem. Commun.*, 2011, **47**, 6689.
- 48 N. Meir, I. J.-L. Plante, K. Flomin, E. Chockler, B. Moshofsky, M. Diab, M. Volokh and T. Mokari, *J. Mater. Chem. A*, 2013, **1**, 1763.
- 49 D.-Y. Liu, S.-Y. Ding, H.-X. Lin, B.-J. Liu, Z.-Z. Ye, F.-R. Fan, B. Ren and Z.-Q. Tian, *J. Phys. Chem. C*, 2012, **116**, 4477.
- 50 L. Kong, W. Chen, D. Ma, Y. Yang, S. Liu and S. Huang, *J. Mater. Chem.*, 2012, **22**, 719.
- 51 L. Zhang, D. A. Blom and H. Wang, *Chem. Mater.*, 2011, **23**, 4587.
- 52 W.-C. Wang, L.-M. Lyu and M. H. Huang, *Chem. Mater.*, 2011, **23**, 2677.
- 53 H. Yin, Z. Ma, M. Chi and S. Dai, *Catal. Today*, 2011, **160**, 87.
- 54 F.-h. Lin and R.-a. Doong, *J. Phys. Chem. C*, 2011, **115**, 6591.
- 55 H. Sun, J. He, J. Wang, S. -Y. Zhang, C. Liu, T. Sritharan, S. Mhaisalkar, M. -Y. Han, D. Wang and H. Chen, *J. Am. Chem. Soc.*, 2013, **135**, 9099.
- 56 S. K. Tripathy, A. Mishra, S. K. Jha, R. Wahab and A. A. Al-Khedhairi, *Anal. Methods*, 2013, **5**, 1456.
- 57 K. Yu, Z. Wu, Q. Zhao, B. Li and Y. Xie, *J. Phys. Chem. C*, 2008, **112**, 2244.
- 58 J. Li, S. K. Cushing, J. Bright, F. Meng, T. R. Senty, P. Zheng, A. D. Bristow and N. Wu, *ACS Catal.*, 2013, **3**, 47.
- 59 T. Mitsudome, Y. Mikami, M. Matoba, T. Mizugaki, K. Jitsukawa and K. Kaneda, *Angew. Chem. Int. Ed.*, 2012, **51**, 136.
- 60 M. E. Aguirre, H. B. Rodríguez, E. S. Román, A. Feldhoff and M. A. Grela, *J. Phys. Chem. C*, 2011, **115**, 24967.
- 61 W. Jiang, Y. Zhou, Y. Zhang, S. Xuan and X. Gong, *Dalton Trans.*, 2012, **41**, 4594.
- 62 R.-J. Wu, D.-J. Lin, M.-R. Yu, M. H. Chen and H.-F. Lai, *Sensor. Actuat. B-Chem.*, 2013, **178**, 185.
- 63 X.-F. Wu, Y.-F. Chen, J.-M. Yoon and Y.-T. Yu, *Mater. Lett.*, 2010, **64**, 2208.
- 64 Z. Zhuang, Q. Peng and Y. Li, *Chem. Soc. Rev.*, 2011, **40**, 5492.
- 65 P. Li, Z. Wei, T. Wu, Q. Peng and Y. Li, *J. Am. Chem. Soc.*, 2011, **133**, 5660.
- 66 H. Yu, M. Chen, P. M. Rice, S. X. Wang, R. L. White and S. Sun, *Nano Lett.*, 2005, **5**, 379.
- 67 W. Shi, H. Zeng, Y. Sahoo, T. Y. Ohulchanskyy, Y. Ding, Z. L. Wang, M. Swihart and P. N. Prasad, *Nano Lett.*, 2006, **6**, 875.
- 68 J. Huang, Y. Sun, S. Huang, K. Yu, Q. Zhao, F. Peng, H. Yu, H. Wang and J. Yang, *J. Mater. Chem.*, 2011, **21**, 17930.
- 69 C. Wang, H. Yin, S. Dai and S. Sun, *Chem. Mater.*, 2010, **22**, 3277.
- 70 C.-H. Kuo, T.-E. Hua and M. H. Huang, *J. Am. Chem. Soc.*, 2009, **131**, 17871.
- 71 C. -H. Kuo, Y. -C. Yang, S. Gwo and M. H. Huang, *J. Am. Chem. Soc.*, 2011, **133**, 1052.
- 72 M. Casavola, R. Buonsanti, G. Caputo and P. D. Cozzoli, *Eur. J. Inorg. Chem.*, 2008, 837.
- 73 X. Zhu, L. Wu, D. C. Mungra, S. Xia and J. Zhu, *Analyst*, 2012, **137**, 2454.
- 74 A. Vanderkooy and M. A. Brook, *ACS Appl. Mater. Interfaces*, 2012, **4**, 3980.
- 75 Z. Bai, R. Chen, P. Si, Y. Huang, H. Sun and D.-H. Kim, *ACS Appl. Mater. Interfaces*, 2013, **5**, 5856.
- 76 B. P. Bastakoti, S. Guragain, S.-i. Yusa and K. Nakashima, *RSC Adv.*, 2012, **2**, 5938.
- 77 L. Rainville, M.-C. Dorais and D. Boudreau, *RSC Adv.*, 2013, **3**, 13953.
- 78 J.-N. Park, A. J. Forman, W. Tang, J. Cheng, Y.-S. Hu, H. Lin and E. W. McFarland, *Small*, 2008, **4**, 1694.
- 79 S. H. Joo, J. Y. Park, C.-K. Tsung, Y. Yamada, P. Yang and G. A. Somorjai, *Nat. Mater.*, 2009, **8**, 126.
- 80 T. D. Schladt, M. I. Shukoor, K. Schneider, M. N. Tahir, F. Natalio, I. Ament, J. Becker, F. D. Jochum, S. Weber, O. Köhler, P. Theato, L. M. Schreiber, C. Sönnichsen, H. C. Schröder, W. E. G. Müller and W. Tremel, *Angew. Chem. Int. Ed.*, 2010, **49**, 3976.
- 81 N. L. Wieder, M. Cargnello, K. Bakhmutsky, T. Montini, P. Fornasiero and R. J. Gorte, *J. Phys. Chem. C*, 2011, **115**, 915.
- 82 N. Zhang, X. Fu and Y.-J. Xu, *J. Mater. Chem.*, 2011, **21**, 8152.
- 83 X. F. Wu, H. -Y. Song, J. -M. Yoon, Y. -T. Yu and Y. -F. Chen, *Langmuir*, 2009, **25**, 6438.
- 84 T. Mitsudome, M. Matoba, T. Mizugaki, K. Jitsukawa and K. Kaneda, *Chem.-Eur. J.*, 2013, **19**, 5255.
- 85 J. Zhang, L. Li, X. Huang and G. Li, *J. Mater. Chem.*, 2012, **22**, 10480.
- 86 H. Hong, L. Hu, M. Li, J. Zheng, X. Sun, X. Lu, X. Cao, J. Lu and H. Gu, *Chem. -Eur. J.*, 2011, **17**, 8726.
- 87 Y. Li, Y. Lu, H. Hong, Y. Chen, X. Ma, L. Guo, Z. Wang, J. Chen, M. Zhu, J. Ni, H. Gu, J. Lu and J. Y. Ying, *Chem. Commun.*, 2011, **47**, 6320.
- 88 J. Liu, S. Z. Qiao, J. S. Chen, X. W. Lou, X. Xing and G. Q. Lu, *Chem. Commun.*, 2011, **47**, 12578.
- 89 X. Fang Z. Liu, M.-F. Hsieh, M. Chen, P. Liu, C. Chen and N. Zheng, *ACS Nano*, 2012, **6**, 4434.
- 90 Z. Wang, L. Zhou and X. W. Lou, *Adv. Mater.*, 2012, **24**, 1903.
- 91 J. Liu, H. Q. Yang, F. Kleitz, Z. G. Chen, T. Yang, E. Strounina, G. Q. Lu and S. Z. Qiao, *Adv. Funct. Mater.*, 2012, **22**, 591.
- 92 K. Kamata, Y. Lu and Y. Xia, *J. Am. Chem. Soc.*, 2003, **125**, 2384.
- 93 I. Lee, J. B. Joo, Y. Yin and F. Zaera, *Angew. Chem. Int. Ed.*, 2011, **50**, 10208.
- 94 R. J. Dillon, J. -B. Joo, F. Zaera, Y. Yin and C. J. Bardeen, *Phys. Chem. Chem. Phys.*, 2013, **15**, 1488.
- 95 X. Huang, C. Guo, J. Zuo, N. Zheng and G. D. Stucky, *Small*, 2009, **5**, 361.
- 96 C. Galeano, R. Güttel, M. Paul, P. Arnal, A. -H. Lu and F. Schüth, *Chem. -Eur. J.*, 2011, **17**, 8434.
- 97 R. Güttel, M. Paul and F. Schüth, *Chem. Commun.*, 2010, **46**, 895.
- 98 P. M. Arnal, M. Comotti and F. Schüth, *Angew. Chem. Int. Ed.*, 2006, **45**, 8224.
- 99 E. V. Shevchenko, M. I. Bodnarchuk, M. V. Kovalenko, D. V. Talapin, R. K. Smith, S. Aloni, W. Heiss and A. P. Alivisatos, *Adv. Mater.*, 2008, **20**, 4323.
- 100 Z. Wei, Z. Zhou, M. Yang, C. Lin, Z. Zhao, D. Huang, Z. Chen and J. Gao, *J. Mater. Chem.*, 2011, **21**, 16344.
- 101 C. Chen, X. Fang, B. Wu, L. Huang and N. Zheng, *ChemCatChem*, 2012, **4**, 1578.
- 102 X. Liang, J. Li, J. B. Joo, A. Gutiérrez, A. Tillekaratne, I. Lee, Y. Yin and F. Zaera, *Angew. Chem. Int. Ed.*, 2012, **51**, 8034.
- 103 Q. Zhang, W. Wang, J. Goebel and Y. Yin, *Nano Today*, 2009, **4**, 494.
- 104 M. Kim, J. C. Park, A. Kim, K. H. Park and H. Song, *Langmuir*, 2012, **28**, 6441.
- 105 L. Wang, H. Dou, Z. Lou and T. Zhang, *Nanoscale*, 2013, **5**, 2686.
- 106 K. Dong, Z. Liu and J. Ren, *CryEngComm*, 2013, **15**, 6329.
- 107 W. Li, Y. Deng, Z. Wu, X. Qian, J. Yang, Y. Wang, D. Gu, F. Zhang, B. Tu and D. Zhao, *J. Am. Chem. Soc.*, 2011, **133**, 15830.
- 108 R. Güttel, M. Paul, C. Galeano and F. Schüth, *J. Catal.*, 2012, **289**, 100.
- 109 Y. J. Wong, L. Zhu, W. S. Teo, Y. W. Tan, Y. Yang, C. Wang and H. Chen, *J. Am. Chem. Soc.*, 2011, **133**, 11422.
- 110 X. -J. Wu and D. Xu, *Adv. Mater.*, 2010, **22**, 1516.
- 111 X. Li, X. Fu and H. Yang, *Phys. Chem. Chem. Phys.*, 2011, **13**, 2809.
- 112 H. C. Zeng, *J. Mater. Chem.*, 2006, **16**, 649.
- 113 H. C. Zeng, *Curr. Nanosci.*, 2007, **3**, 177.
- 114 J. Du, J. Qi, D. Wang and Z. Tang, *Energy Environ. Sci.*, 2012, **5**, 6914.
- 115 Y. Yin, R. M. Rioux, C. K. Erdonmez, S. Hughes, G. A. Somorjai and A. P. Alivisatos, *Science*, 2004, **304**, 711.
- 116 H. J. Fan, U. Gösele and M. Zacharias, *Small*, 2007, **3**, 1660.
- 117 J. Gao, G. Liang, J. S. Cheung, Y. Pan, Y. Kuang, F. Zhao, B. Zhang, X. Zhang, E. X. Wu and B. Xu, *J. Am. Chem. Soc.*, 2008, **130**, 11828.
- 118 Y. Chen, B. Zhu, M. Yao, S. Wang and S. Zhang, *Catal. Commun.*, 2010, **11**, 1003.
- 119 Q. Fu, W. -X. Li, Y. Yao, H. Liu, H. -Y. Su, D. Ma, X. -K. Gu, L. Chen, Z. Wang, H. Zhang, B. Wang and X. Bao, *Science*, 2010, **328**, 1141.
- 120 H. Zhang, Y. Wang, P. Liu, Y. Han, X. Yao, J. Zou, H. Cheng and H. Zhao, *ACS Appl. Mater. Interfaces*, 2011, **3**, 2472.
- 121 Y. Wang, T. Sun, D. Yang, H. Liu, H. Zhang, X. Yao and H. Zhao, *Phys. Chem. Chem. Phys.*, 2012, **14**, 2333.

- 122 R. Güttel, M. Paul and F. Schüth, *Catal. Sci. Technol.*, 2011, **1**, 65.
- 123 M. Haruta, N. Yamada, T. Kobayashi and S. Iijima, *J. Catal.*, 1989, **115**, 301.
- 124 F. Boccuzzi, A. Chiorino, M. Manzoli, P. Lu, T. Akita, S. Ichikawa and M. Haruta, *J. Catal.*, 2001, **202**, 256.
- 5 125 X. Liu, M. -H. Liu, Y. -C. Luo, C. -Y. Mou, S. D. Lin, H. Cheng, J. -M. Chen, J. -F. Lee and T. -S. Lin, *J. Am. Chem. Soc.*, 2012, **134**, 10251.
- 126 X.-J. Liu, C.-H. Cui, M. Gong, H.-H. Li, Y. Xue, F.-J. Fan and S.-H. Yu, *Chem. Commun.*, 2013, **49**, 8704.
- 10 127 Q. Gao, Y.-M. Ju, D. An, M.-R. Gao, J.-W. Liu, C.-H. Cui and S.-H. Yu, *ChemSusChem*, 2013, **6**, 1878.
- 128 B. Y. Xia, H. B. Wu, X. Wang and X. W. Lou, *J. Am. Chem. Soc.*, 2012, **134**, 13934.
- 15 129 X.-H. Guo, C.-C. Mao, J. Zhang, J. Huang, W. -N. Wang, Y. -H. Deng, Y. -Y. Wang, Y. Cao, W.-X. Huang and S.-H. Yu, *Small* 2012, **8**, 1515.

20



Guodong Li received his BS degree from University of Jinan in 2004, MS degree from Ocean University of China in 2007, and PhD degree from Beijing University of Chemical Technology in 2011. Then, he joined Prof. Zhiyong Tang's group in National Center for Nanoscience and Technology. His current research interests are focused on fabrication of inorganic nanocomposites with well-defined structures as well as their application in catalysis.



Zhiyong Tang obtained his PhD degree in 1999 from Chinese Academy of Sciences. After this, he went to Swiss Federal Institute of Technology Zurich and University of Michigan for his postdoctoral research. In November of 2006, he joined National Center for Nanoscience and Technology in China and took up a full professor position. Zhiyong Tang's current research interests are focused on fabrication and application of chiral inorganic nanoparticles as well as nanoparticle superstructures.